Path-based blast loading in urban environments

Jurre Knijff

Delft University of Technology

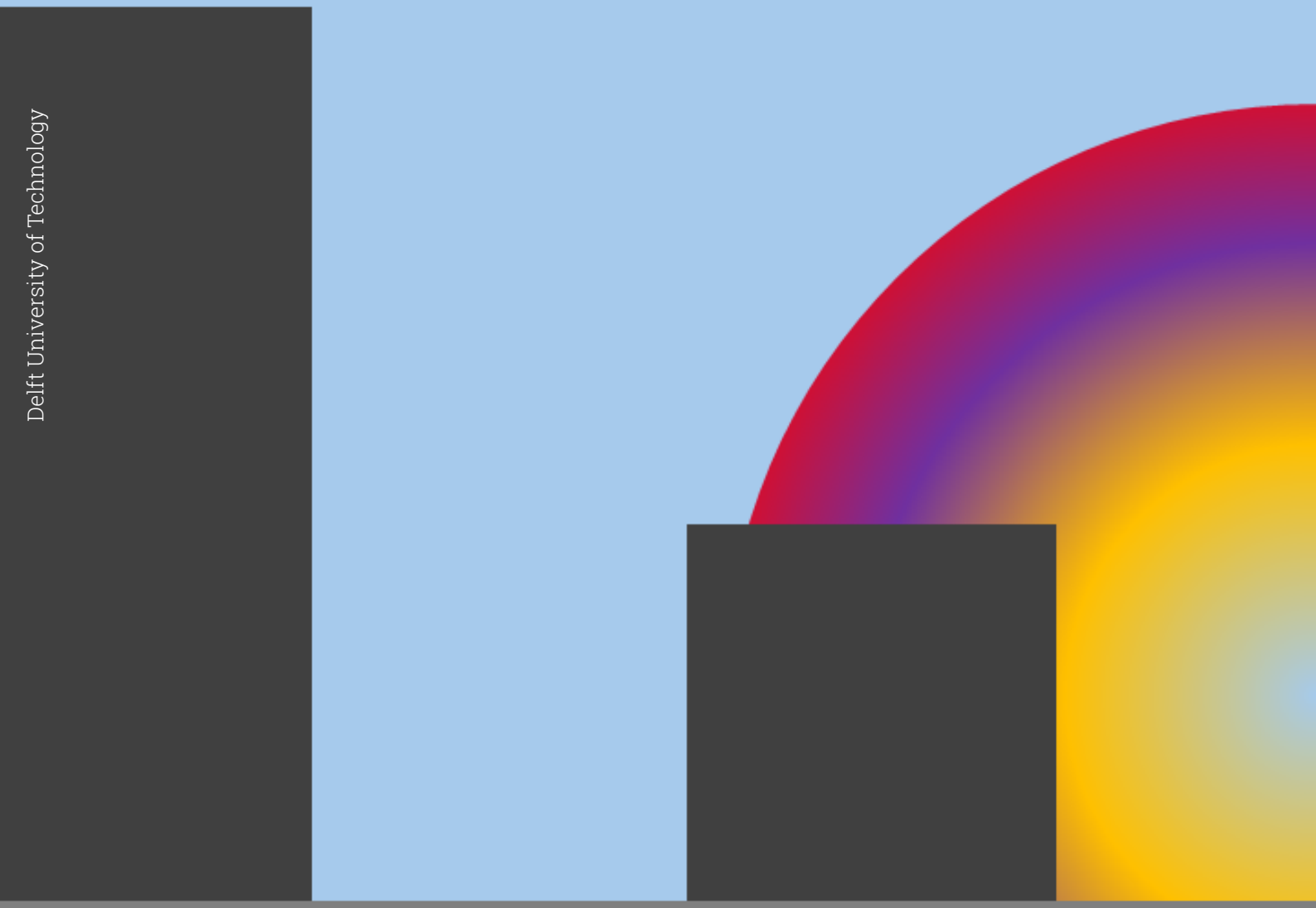

TU Delft

TNO

Path-based blast loading in urban environments

by

Jurre Knijff

to obtain the degree of Master of Science
at the Delft University of Technology,

Student number:	4489470	
Thesis committee:	Dr. P. C. J. Hoogenboom	TU Delft, supervisor
	Ir. A. C. B. Schuurman,	TU Delft
	Dr. Ir. F. F. J. Schrijer	TU Delft
	Ir. H. P. A. Dijkers	TNO

Style: TU Delft Report Style, with modifications by Daan Zwaneveld

An electronic version of this thesis is available at http://repository.tudelft.nl/.

TU Delft

TNO

Preface

This thesis is the end result of research into path-based loading models and the final stage of my master's at TU Delft. The final stretch of the thesis has taken much longer than intended, and I could not have completed it without the help of many people. First of all, I would like to thank Hugo Dijkers for his daily supervision at TNO and for giving me the opportunity to visit some of the more restricted locations within TNO. I would also like to thank everyone at the Ypenburg location for their interest in my research and for the nice atmosphere. Secondly, I would like to thank Marco Schuurman, Pierre Hoogenboom, and Ferry Schrijer not only for the help and insights on all the subjects covered in this thesis, but also for their continued support throughout this thesis, even after months of silence. I also want to thank Wouter Halswijk for his explanation on the original version of BeamBlast, and Jelme Pennings for his help on the CFD simulations and his guidance on using Apollo.

Last, I want to thank my friends, family and girlfriend for their support throughout the whole length of my thesis and studies, without whom I would not have been able to complete this thesis.

Jurre Knijff
Delft, May 2026

Summary

Due to the transport of dangerous liquids through city centres in the Netherlands by train, buildings in urban areas can be subject to explosion loading. Loading due to explosions has to be taken into account in structural engineering to ensure the safety of users of buildings. However, using computer software for this task is often difficult, due to its steep learning curve, complex inputs and long computation time. This thesis looks into the possibility of using a path-based loading model to simplify and speed up this computation, such that a first estimate of the loading conditions can be found quickly. An existing path-based loading model called BeamBlast was used, which creates blast loading paths based on the geometry of the environment, the location of the blast, and the location at which the blast loading is relevant, referred to as the subject location. When these paths are combined with the explosive mass, BeamBlast returns the maximum pressure and positive impulse at the subject location. From the paths, BeamBlast finds the ”events” along a path, such as reflections, diffractions and clearing effects. Based on the effects, the maximum pressure and wave shape are changed, such that the wave shape is corrected for the event that occurs. Using research, multiple approaches were applied and compared to find the best method for each of the effects. An experimental setup was modelled both in CFD and BeamBlast, which showed that BeamBlast suffers from certain effects, such as ground explosions and wall subjects. However, using BeamBlast, the pressure and impulse were calculated much faster compared to a CFD analysis, with a time gain of around a factor of 1000 for a small T-Junction. In an urban case study with more complex geometry, the path-based model will be slower. The urban case study, where multiple buildings were placed and the blast was located asymmetrically with respect to the buildings, took around 8 minutes to complete using BeamBlast. A CFD was attempted, but not completed due to time constraints. To conclude, a path-based loading model can be much faster than CFD at the current time, while also retaining accuracy, making it applicable for early design stage applications. However, it is recommended that more research needs to be done into the edge effects and their equations, as well as a more complex comparison between BeamBlast and CFD to fully test the capability of BeamBlast.

Contents

Preface i

Summary ii

List of Symbols v

1 Introduction 1
- 1.1 General overview . . . 1
- 1.2 Research aim . . . 2
- 1.3 Research Methodology . . . 2
- 1.4 Thesis outline . . . 2

2 Literature research 4
- 2.1 Blast waves . . . 4
- 2.2 Blast wave equation . . . 5
  - 2.2.1 Explosion parameters . . . 6
- 2.3 Blast wave interaction . . . 8
  - 2.3.1 Reflections . . . 9
  - 2.3.2 Diffraction of blast waves . . . 11
  - 2.3.3 Clearing pressure . . . 16
  - 2.3.4 Other edge effects . . . 17
- 2.4 Predicting explosion damage . . . 19

3 BeamBlast 21
- 3.1 Structure and input . . . 21
  - 3.1.1 Input . . . 22
  - 3.1.2 Path finding . . . 22
  - 3.1.3 Blast load generation . . . 22
- 3.2 Original Blast Loading . . . 23
  - 3.2.1 Structure . . . 23
  - 3.2.2 Reflections and edge effects . . . 23
  - 3.2.3 Wave parameters . . . 23
  - 3.2.4 Wave shape . . . 23
- 3.3 Modified Blast Loading . . . 24
  - 3.3.1 Structure . . . 24
  - 3.3.2 Wave parameters . . . 24
  - 3.3.3 Initial phase . . . 24
  - 3.3.4 Reflection . . . 25
  - 3.3.5 Diffraction . . . 25
  - 3.3.6 Edge Reflection . . . 25
  - 3.3.7 Clearing . . . 25
- 3.4 Verification . . . 25
  - 3.4.1 Blast wave equation and scaled distances . . . 25
  - 3.4.2 Clearing pressure . . . 25
  - 3.4.3 Diffraction . . . 27
  - 3.4.4 Edge events . . . 29
- 3.5 Discussion . . . 29

4 General case study 30
- 4.1 Physical problem . . . 30
- 4.2 Initial conditions . . . 30

4.3 BeamBlast . . . 31
4.4 CFD analysis . . . 31
4.5 Results . . . 31
4.6 Discussion . . . 31

5 Urban case study **33**
5.1 Physical problem and mechanical model . . . 33
5.2 Mechanical model . . . 33
5.3 BeamBlast input . . . 34
5.4 Results . . . 34
5.5 Discussion . . . 34

6 Conclusion and recommendations **37**
6.1 Conclusion . . . 37
6.2 Recommendations . . . 37

References **41**

List of Symbols

Latin Symbols

c_0	Speed of sound in standard air
d	Decay parameter
E	Enthalpy
H	Specific Enthalpy
M	Mach number of shock wave
p_{smin}	Minimum underpressure
p_{so}	Maximum overpressure
P_0	Standard air pressure
q	Dynamic pressure
t_a	Arrival time of the pressure wave
t_d	Positive duration of the pressure wave
t_d^-	Negative duration of the pressure wave
u	Shockwave speed
W	Mass of the explosion

Greek Symbols

γ	Specific density of air
ΔP	Overpressure
ξ	Inverse shock strength
ρ	Air density

1

Introduction

1.1. General overview

In the past years, the Dutch news has been prominently featuring more and more explosions, almost exclusively caused by criminal activities. In 2025, there were 1356 explosions, specifically targeting houses and businesses (NOS, 2025). Although most of these explosions have not led to large structural damage, the explosion occurring at the Tarwekamp (The Hague) shows that large structural failure can occur. This explosion, which occurred in 2024, caused six casualties and left four wounded (Ministerie", n.d.). Other past events around the world, such as the Paris Bombings in 2015, the Brussels bombings in 2016, and the Oklahoma bombing in 1995, show that these attacks are carried out in urban areas around the world. The Oklahoma bombing has been one of the largest explosions in an urban area, which resulted in the death of 168 people (FBI, n.d.). Another example of a cause of explosions included industrial explosions of trains, containing industrial gases and liquids. Although the probability of explosions and accidents with flammable liquids transported by train is small, the accident in East-Palastine (Ohio, United States) (NOS, 2023) show that these kind of explosions should be accounted for. Moreover, in 2009, an accident with a LPG-loaded train occurred in Viareggio, where 14 people were killed after a train derailment followed by an LPG explosion (Trouw, 2009). In the Netherlands, spaces close to train tracks are more often chosen for the development of buildings. Some of these tracks facilitate the transport of industrial traffic, of which some are highly flammable gases and liquids. The number of transports with highly flammable gases has increased over the past years (AVIV, 2021), which even go through urban areas in Noord-Brabant, such as Breda, Eindhoven, and Tilburg (Kenniscentrum InfoMil van Rijkswaterstaat, 2020).

To take the possibility of such events into account in building design, loading conditions due to explosions need to be taken into account. To be able to make a good estimation of the price of a building, these loads should be taken into account during variant studies or in the early design stages. However, the time and money spent on these stages of design should be small, since it is not certain that a return of investment is guaranteed. This is in stark contrast with the possibility of underestimating the loading conditions and having a smaller return of investment in the long term, due to an overestimation of the possible profit. However, due to the conditions of other buildings and objects in the vicinity of the new building, the load might be different compared to a 'free field' blast, where the explosion can be estimated using distance scaling and surrounding objects are not considered.

When considering the surrounding objects and buildings, the surroundings should be modelled up to a certain level of detail. These environmental models have been more and more available, such as the 3DBAG models, OSM buildings, Cesium, and many other, which uses LIDAR (Laser Imaging Detection And Ranging) to make three-dimensional models of the Netherlands. City4CFD extends the 3DBAG in terms that City4CFD does not contain the elevation as surfaces, which allows reflections. Using these models, the blast load on a building phase can be estimated by using CFD, which can accurately predict the load on a building. However, these CFD models, especially when considering bigger environments, can have a very high run time and need a good understanding of the concepts that are introduced into

these models. Therefore, this thesis looks into another way to predict the explosion load on the face of a building, considering the environment, while being faster than CFD.

1.2. Research aim

The aim of this master thesis is to look into the possibility of using a path-based blast loading model to predict and analyse blast wave propagation through an urban environment. The blast wave propagation can be used to predict the load and damage due to an explosion in a complex urban environment on an existing building or a new structure. The method will be compared to an CFD analysis to determine its applicability within preliminary building design. This thesis will focus on large scaled distances, where standard blast scaling relations can be used. The path based loading model will be compared to a CFD analysis in terms of speed and accuracy of the results. The master thesis will use an existing path-based loading model called BeamBlast, developed by Halswijk (2015). BeamBlast is an existing path based loading model made in MATLAB, which bases the paths on a geometry input by the user, and gives output based on the paths and explosion mass. The path-finding method will not be modified, only the calculation of the effects of the blast will be modified. The modification in the effects calculation will be done based on literature research. Therefore, this thesis will feature both the original version of BeamBlast, as well as a modified version. To guide this research, the following questions have been formulated:

- What output is relevant to evaluate the behaviour and damage of the environment and how can this be communicated?
- What input and relations are needed to determine the output of the path based model?
- How do the results of a path based loading models compare to CFD in terms of speed and accuracy?

1.3. Research Methodology

The first question will go into the damage of explosions and the possible damage models that can be used to estimate the damage done by a blast load. This will go into the output that is needed from software to give an estimation of the damage.

The second question will go into the different paths that an explosion wave can travel, and how these paths and objects along the path influence the output results that have been found from the first question. This question will be based on literature research and will compare the BeamBlast outcome to different experiments.

The third question will be answered by doing two analyses. One of the analyses will be on the verification side, such that both the results of CFD and the path-based loading model can be compared with an experiment, while comparing the two computational methods in terms of speed. The second analysis will contain a more urban model to show the capability of the path-based loading model and compare both the original version and the modified version.

1.4. Thesis outline

Chapter 2 will go into the behaviour of blast waves in general, as well as looking into their interactions with edges and surfaces. With this, a number of equations will be mentioned that will be used to test the methods in path-based loading models.

The third chapter will go into BeamBlast itself, in which the original version and modified version are explained in terms of how they consider objects along their path. The modified version will contain multiple different methods. Both the original and modified versions of BeamBlast will be compared to experimental data, such that different methods can be compared to experimental results.

Chapter 4 will use both versions of BeamBlast into a more complex environment to test the speed and accuracy of the path-based loading model, while also comparing the results of an CFD analysis to the experimental data.

Chapter 5 will feature an application to an urban situation, containing multiple buildings. This section

will again use both the original and modified version, such that the speed and output of the original and modified path-based loading model can be shown.

2

Literature research

2.1. Blast waves

A blast wave can be described as a shock wave moving through a medium. Although blast waves can have different shapes and sizes, the common thing between the terms is a pressure difference between the air before and after the blast. This pressure difference can be seen in figure 2.1, which shows the pressure development over time for a hemispherical explosion (Sielicki & Rigby, 2014). From figure 2.1, in which the overpressure is the air pressure above atmospheric pressure, it can be seen that there is a large and sudden jump in the pressure before and after the arrival of the blast wave.

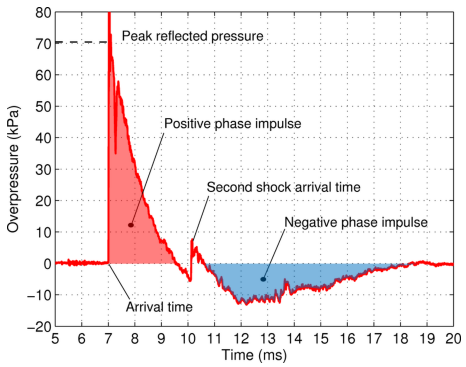

Figure 2.1: Experimental pressure time curve for a hemispherical explosion (Sielicki & Rigby, 2014), with the positive impulse in the red region and the negative impulse in the blue region

In figure 2.1, the positive phase impulse is equal to the integration of pressure over the positive duration, while the negative impulse is equal to the integration of negative pressure over the negative duration. The jump in pressure does not only occur for pressure, but applies to the density and velocity as well. For general problems in gas dynamics, continuity equations are used (Bakker & van Leer, 2019). These relate the conditions of flow, such as density, pressure and velocity, to each other using conservation of mass, momentum and energy. However, these equations cannot be used directly, due to the earlier-mentioned 'jump' in their properties. The continuity equations describe the relation between pressure, temperature and density. The conservation equations include conservation of mass, momentum and energy. To take into account the jump in pressure and velocity, the Rankine-Hugoniot relations can be used:

$$\rho_1 u_1 = \rho_2 u_2 \tag{2.1}$$

$$p_1 + \rho_1 u_1^2 = p_2 + \rho_2 u_2^2 \tag{2.2}$$

$$\rho_1 u_1 H_1 = \rho_2 u_2 H_2 \tag{2.3}$$

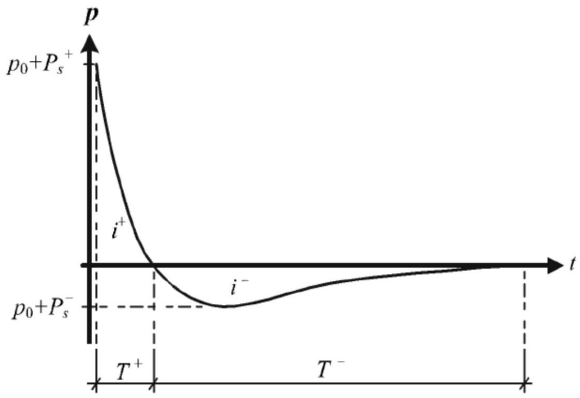

Figure 2.2: Ideal blast wave (Tavakoli & Kiakojouri, 2014)

with ρ as the density, u as the gas velocity, p the pressure and H the total specific enthalpy. For the specific energy, the following equation is used:

$$H = E + \frac{p}{\rho} \tag{2.4}$$

From the Rankine-Hugueniot equations, the following relations can be derived (Bakker & van Leer, 2019).

$$M_1 = \sqrt{1 + \frac{\gamma+1}{2\gamma}\frac{p_2 - p_1}{p_1}} \tag{2.5}$$

$$\rho_2 = \rho_1 \frac{(\gamma+1)M_1^2}{2 + (\gamma-1)M_1^2} \tag{2.6}$$

$$u_2 = u_1 \left(1 - \frac{2}{\gamma+1}\frac{M_1^2 - 1}{M_1^2}\right) \tag{2.7}$$

Using these relations and knowing the pressure at a location and time, the Mach number, density and flow velocity can be calculated.

2.2. Blast wave equation

The blast wave shown in figure 2.2 has been described by Friedlander and Taylor (1946), which has been modified by Dewey (2018) and can be found as equation 2.8. Equation 2.8 is known as the modified Friedlander equation, describing the pressure over time based on distance and TNT mass.

$$p_s(t) = p_{so}\left(1 - \frac{t}{t_d}\right)e^{-dt/t_d} \tag{2.8}$$

In equation 2.8, p_s is the pressure at the location over time, p_{so} is the peak pressure, t_d is the positive duration of the blast wave and d is known as the parameter that determines the rate of decay. Figure 2.2 shows a representation of an ideal blast wave.

Although equation 2.8 describes the positive phase of a blast wave well, for the negative phase, in which the overpressure is lower than the ambient pressure, experimental validation of the negative phase has not been done often (Rigby, Tyas, Bennett, Clarke, & Fay, 2014). From Rigby et al. (2014), it can be found that a cubic line follows the behaviour of the experiment more closely in the case of negative pressure. The cubic negative can be described using equation 2.9 (Granström, 1956), which closely fits experimental data points (Rigby et al., 2014).

	Near field			Far field		
Energetic	Average pressure (kPa)	Coefficient of variation (%)	TNT Equivalence	Average pressure (kPa)	Coefficient of variation (%)	TNT equivalence
TNT	196.8	2.89	1.00	21.81	10.5	1.00
Helix	188.8	6.83	0.96	23.42	4.06	1.07
Texpak	150.2	9.72	0.76	19.49	9.18	0.89
Kinepak	69.85	1.80	0.35	12.75	4.00	0.58
Rimfire	79.73	5.00	0.41	14.33	3.49	0.66
Rimfire (L)	76.52	6.56	0.41	14.32	10.3	0.66
Tannerite (L)	75.44	3.02	0.40	12.58	9.46	0.57

Figure 2.3: TNT Equivalence of a number of energetic materials (James et al., 2025)

$$p_s(t) = -p_{s,min}\frac{6.75(t-t_d)}{t_d^-}\left(1-\frac{t-t_d}{t_d^-}\right)^2 \tag{2.9}$$

When combining both equations, the total equation for pressure over time can be written according to equation 2.10. It has to be noted that this equation is truncated at the end of the negative phase.

$$p(t) = \begin{cases} p_{so}\left(1-\frac{t}{t_d}\right)e^{-dt/t_d}, & 0 \le t \le t_d \\ -p_{s,min}\frac{6.75(t-t_d)}{t_d^-}\left(1-\frac{t-t_d}{t_d^-}\right)^2, & t_d < t \le t_d + t_d^- \\ 0, & \text{otherwise} \end{cases} \tag{2.10}$$

2.2.1. Explosion parameters

To be able to compare explosions of different sizes and distances, scaling laws can be used. One of these scaling laws has been developed by Hopkinson (1915), which can be seen in equation 2.11. In equation 2.11, W is the energy of the explosive and R the distance to the target. In most cases, W represents the total mass of TNT, since energy is proportional to the total mass (Baker, 1973).

$$Z = \frac{L}{W^{\frac{1}{3}}} \tag{2.11}$$

To simplify and generalize the equations for explosions and its effects, the concept of TNT equivalence is used. A TNT equivalence is expressed as the ratio between the heat of detonation of any explosive and the heat of explosion of TNT. Equation 2.12 is used for the conversion, where W is the true mass, H is the heat of detonation for the explosive and H_{TNT} is the heat of detonation for TNT.

$$W_{eq} = W\frac{H}{H_{TNT}} \tag{2.12}$$

The mass of any explosive can then be expressed as an equivalent TNT mass. An example of the TNT-equivalence of some energetic materials is given in figure 2.3.

Using the equivalent TNT mass, important parameters such as pressure, impulse, and arrival time can be determined without having to implement different equations for different explosives or a combination of explosives. The ratio of H and H_{TNT}, which is referred to as the TNT equivalence of an explosive, is generally described as constant. However, Fuchs, Covino, and Baker (2018) show that this ratio is not constant, but can be dependent on the scaled distance Z. The difference can be found both in the peak pressure, as well as the impulse of the explosion. The difference in TNT equivalence can also be seen in figure 2.3, where the TNT equivalence was different for a 'near field' or 'far field' explosion. Figure 2.3 only shows the comparison of the average pressure, and James et al. (2025) concluded that the TNT equivalence can be different based on the type of output that is monitored.

Having a continuous relation for the blast wave, which has been described in equation 2.10, the pressure can be described over time, given p_{so}, t_d, d, $p_{s,min}$ and t_d^-. Using the scaled distance Z, these properties, except for the decay parameter d, can be determined based on (Kingery & Bulmash, 1984) and Joint Research Centre and Institute for the Protection and Security of the Citizen, Karlos, Viaccoz,

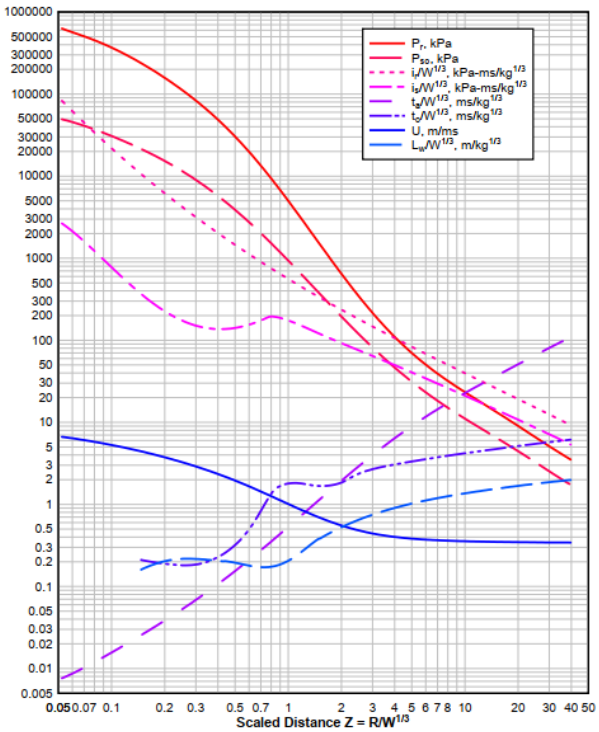

Figure 2.4: Kingery Bulmash parameters for a spherical blast versus scaled distance Z (Joint Research Centre and Institute for the Protection and Security of the Citizen et al., 2013)

and Solomos (2013). Kingery and Bulmash have done multiple tests and provided equations to determine p_{so}, t_d, $p_{s,min}$ and t_d^- based on the scaled distance Z. Figure 2.4 shows the scaled distance Z on the x-axis, and the peak overpressure P_{so}, positive duration t_d and arrival time t_a on the y-axis. According to Kingery and Bulmash (1984), these relations are valid for scaled distances above 0.053 $m/kg^{1/3}$.

Kingery and Bulmash have followed the same procedure for the negative blast wave parameters $p_{r,min}$ and t_d^-. These can also be based on the scale distance, which are shown in figure 2.5.

The Kingery Bulmash relations in figure 2.4 do not show the decay parameter based on the scaled distance. To determine the blast wave decay parameter for scaled distances, Karlos, Larcher, and Solomos (2015) have derived an equation using polynomial fitting. This has been done using a large combination of stand-off distances and charge mass, for which the positive duration, overpressure and impulse were collected based on the scaled distance from Department of Defense (2008). The

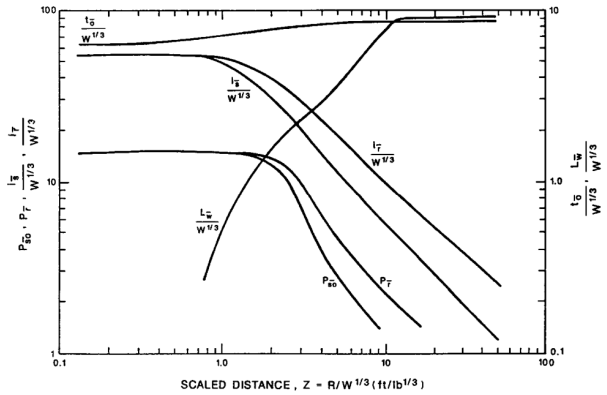

Figure 2.5: $p_{r,min}$ and t_d^- based on scale distance (Department of Defense, 2008)

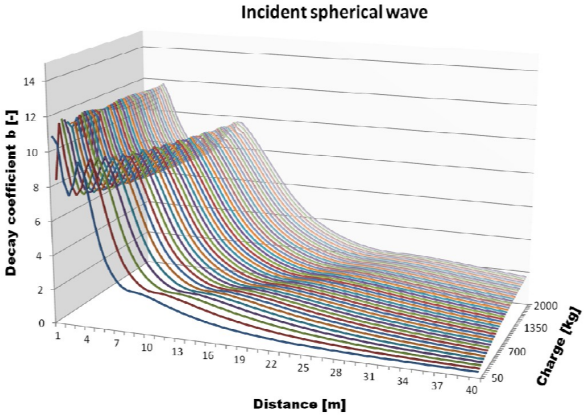

Figure 2.6: Incident spherical wave decay coefficient by using the Kingery-Bulmash data and the Friedlander equation (Karlos et al., 2015)

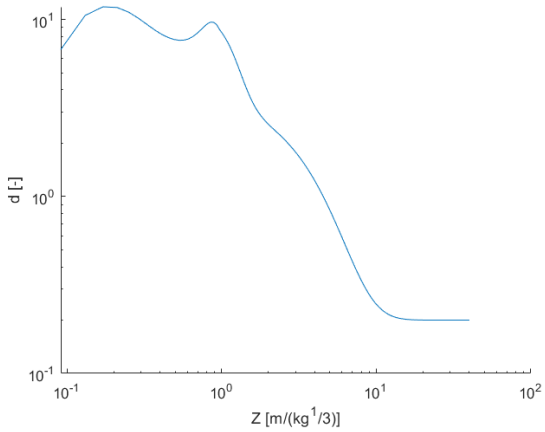

Figure 2.7: Relation between decay coefficient d and scaled distance Z according to equation 2.13

positive duration, overpressure and impulse are then inserted into equation 2.10. Using the pressure and impulse, the decay parameter can be found. This way, the blast wave decay coefficient can be derived from a single curve, such that it can directly be found from the scaled distance, for which the relation is given in equation 2.13. The relation in equation 2.13 is also shown in figure 2.6.

$$d(Z) = \begin{cases} -22.35 + 569.23 * Z - 3657.05 * Z^2 + \\ +11895.32 * Z^3 - 22101.20 * Z^4 + 23778.69 * Z^5 + \\ -13737.89 * Z^6 + 3283.57 * Z^7, & 0.15 < Z < 1.0 \\ 0.20 + 13.77 \left(\frac{0.55}{1+\exp(\frac{Z-1.13}{0.18})} + \frac{1-0.55}{1+\exp(\frac{Z-1.04}{1.83})} \right), & 1.0 < Z < 40.0 \end{cases} \tag{2.13}$$

2.3. Blast wave interaction

There are multiple types of interactions a blast wave can have with either a solid object. An overview of these effects is shown in figure 2.8, where the solid red line is an arriving blast wave and the solid object is shown in gray. The red line is a perfect reflection, which is reflected on the front edge of the object, with its normal vector shown as a dark dotted line. The effect of reflections will be given in chapter 2.3.1. The dark red dotted line is the continuation of the original blast wave, on which the edge has no influence. In the area between the front side and the reflection clearing occurs. Between the back of the objects and the continuation of a blast wave, there will be an area in which diffraction occurs. The other areas, away from the edge, are noted as forward and back edge effects, which will be discussed

at the end of this chapter.

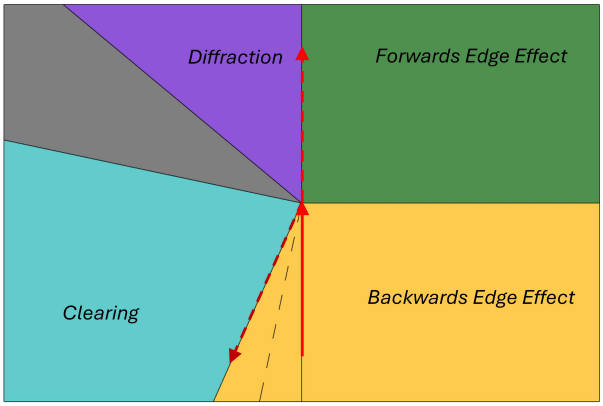

Figure 2.8: Different regions for each of the effects that an edge can have on a blast wave, with the object in gray and the edge located in the centre

2.3.1. Reflections

Reflections occur when a blast wave hits a solid object, after which the blast wave reflects on the surface and creates a reflected overpressure on the surface. This thesis considers a perfect reflection, such that the angle of incidence is equal to the angle of reflection. These reflections are not only important for buildings, but can also be introduced by the ground. Using the Rankine-Hugoniot relations, Needham (2017) has derived an equation for the reflected pressure based on shock wave pressure and specific heat of gas for shock waves which arrive perpendicular to an object. Needham starts by defining the pre-shock state as the ambient pressure P_0, the ambient density ρ_0, temperature T_0 and the ambient material velocity u_0, which is assumed to be 0. The properties of the shock front are described by the pressure P, density ρ, temperature T and material velocity u. The overpressure is defined as:

$$\Delta P = P - P_0 \tag{2.14}$$

The overpressure is used as one of the main properties of the shock front. The density at the shock front is calculated using equation 2.15:

$$\frac{\rho}{\rho_0} = \frac{2\gamma + (\gamma+1)\frac{\Delta P}{P_0}}{2\gamma + (\gamma-1)\frac{\Delta P}{P_0}} \tag{2.15}$$

$$u = \frac{\Delta P}{\gamma P_0} \frac{C_0}{\left(1 + \frac{[\gamma+1]\Delta P}{2\gamma P_0}\right)^{1/2}} \tag{2.16}$$

with C_0 as the speed of sound in the ambient gas, which can be calculated using:

$$C_0 = \sqrt{\gamma P_0 / \rho_0} \tag{2.17}$$

The magnitude of the dynamic pressure is defined as:

$$q = 0.5\rho u^2 \tag{2.18}$$

Equation 2.16 can be used in equation 2.18, which can be rewritten using equation 2.15.

$$q = \frac{\Delta P^2 \frac{C_0^2 \rho_0}{\gamma P_0}}{2\gamma P_0 + (\gamma-1)\Delta P} \tag{2.19}$$

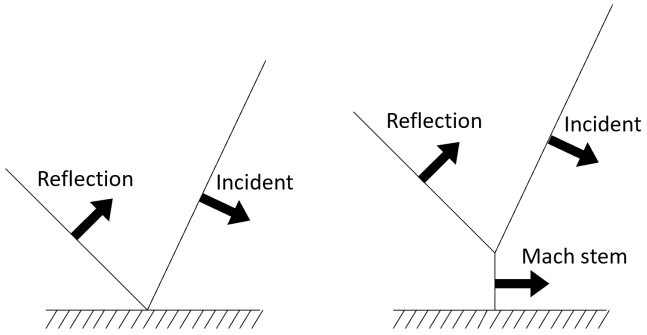

(a) Regular Reflection **(b)** Mach Reflection simplification

Figure 2.9: Different reflection types

Finally using equation 2.17, the dynamic pressure is reduced to:

$$q = \frac{\Delta P^2}{2\gamma P_0 + (\gamma - 1)\Delta P} \tag{2.20}$$

The dynamic pressure is used in combination with the overpressure to find the reflected pressure:

$$\Delta P_r = 2\Delta P + (\gamma + 1)q \tag{2.21}$$

This leads to the reflected pressure of the shockwave:

$$p_r = 2\Delta P \frac{4\gamma P_0 + (3\gamma - 1)\Delta P}{4\gamma P_0 + 2(\gamma - 1)\Delta P} \tag{2.22}$$

Within this thesis, it is assumed that the ration of specific heat is equal to 1.4, which is true for pressures lower than 2000 kPa (Needham, 2017).

$$\Delta P_r = 2P \frac{7P_0 + 4P}{7P_0 + P} \tag{2.23}$$

According to equation 2.23, the reflected pressure can vary between 2 and 8 times the original pressure when for γ value of 1.4 is used.

The above equations are derived for a blast wave arriving perpendicular to the object. For obliquely arriving pressure waves, such as an angled building or a sloping ground, the type of reflection depends on the incidence angle α_I and dimensionless overpressure. Two main types of reflections can occur: a regular reflection or a Mach reflection. The different reflections are shown in figure 2.9. A regular reflection occurs when a reflection bounces off a surface with the same horizontal speed as the incident wave. When the speed of the reflection wave is higher than the incident wave, the reflecting wave overtakes the incident wave, after which a Mach stem occurs (Ben-Dor, 2007). The Mach reflections will be treated at the end of this section. According to Harlow and Amsden (1971) the type of reflection can be based on the inverse shock strength ξ and a relative overpressure. The inverse shock strength ξ can be described using equation 2.24:

$$\xi = \frac{p_0}{p_s + p_0} \tag{2.24}$$

The dimensionless overpressure can be described using equation 2.25:

$$\bar{P_s} = \frac{P_s}{P_0} = \frac{1}{\xi} - 1 \tag{2.25}$$

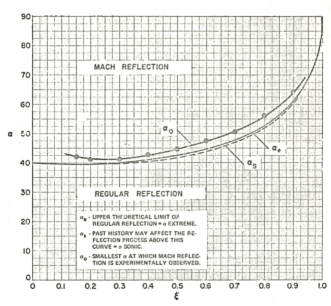

Figure 2.10: Classification of oblique reflection types, where $\gamma = 1.4$ (Harlow & Amsden, 1971)

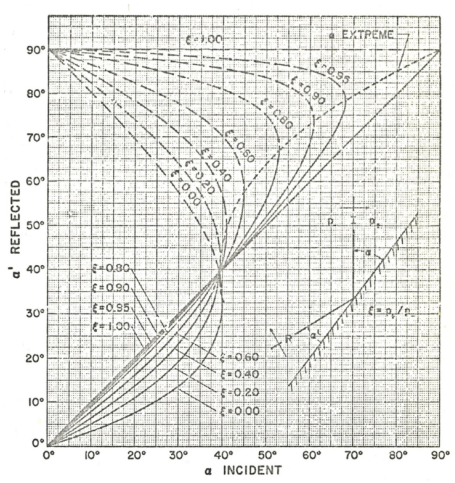

Figure 2.11: Angle of reflection based on incidence angle and inverse shock strength (Harlow & Amsden, 1971)

Figure 2.10 shows whether a reflection can be classified as a regular reflection or as a Mach reflection. For strong shock waves, where the value of ξ is close to 0, it can be found that a Mach reflection will occur when the angle of incidence is higher than 40 degrees. For weak shock waves, with a ξ value closer to 1, a Mach reflection will never occur.

Figure 2.11 shows the reflection angle based on the inverse shock strength and incident angle.

However, in this thesis it was assumed that the reflected angle is equal to the incidence angle. Based on figure 2.11, it can be seen that this is only true for high values of ξ, such that the shock wave is relatively weak.

The reflected over-pressure for both oblique reflections and Mach reflections can be found using figure 2.12, which is based on Glasstone (1962).

Although it was mentioned that for Mach reflections a Mach stem occurs along the wall, this is a simplification of all the scenarios that could occur. For some Mach reflections, vortexes will exist in the reflected region. For simple Mach reflections, such as the one shown in figure 2.9.b, there is a Mach stem which propagates alongside the wall. This Mach stem rises from the wall to a point commonly known as the triple point, above which no Mach stem will occur.

2.3.2. Diffraction of blast waves

When blast waves travel into a more open area than before, a diffraction is caused. Diffraction causes the blast wave to both weaken locally, while creating overpressure in a new direction. A diffraction is shown in figure 2.13, where a weak shockwave is propagating towards the right.

Figure 2.13 shows the shockwave continuing towards the right. Figure 2.13 also shows a radiating pattern expanding downwards along the wall and into the region of post-shockwave state. Three methods for describing diffraction analytically were analysed within this thesis.

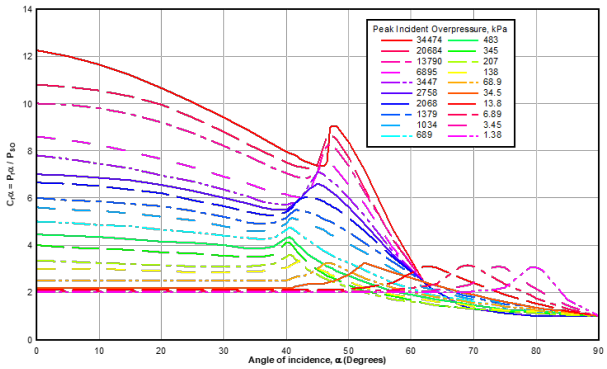

Figure 2.12: Reflection factors as a function of the incident angle for several pressure levels (Department of Defense, 2008)

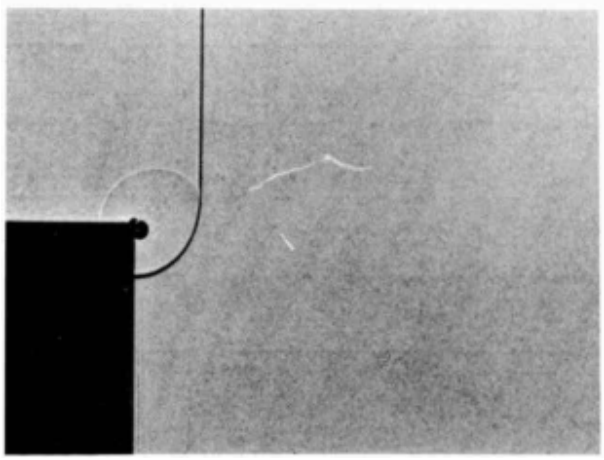

Figure 2.13: Schlieren imaging of a weak shockwave propagating towards the right, while diffracting in a circular pattern when moving into the wider region after the obstacle(Van Dyke, 1982)

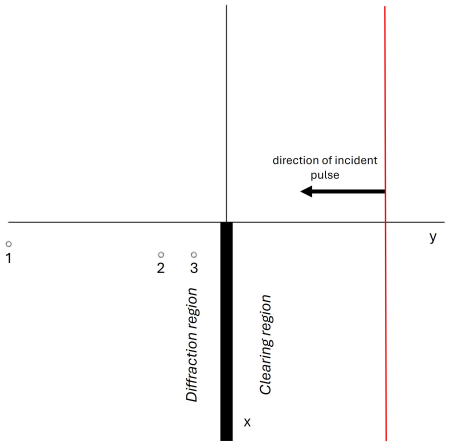

Figure 2.14: Regions defined by Friedlander and Taylor to analyse pulses around a semi-infinite screen(Friedlander & Taylor, 1946), with the wave front shown as the red line

Friedlander method

The first method which has been looked at is referred to as the Friedlander method. Friedlander and Taylor (1946) investigated the diffraction of sound waves, based on earlier work by Sommerfeld (1896) and Lamb (1906). Sommerfeld (1896) focused in their work on the interaction of a wave train and a semi-infinite screen, while Lamb (1906) focused on the interaction of a pulse and a semi-infinite screen. All these researches focussed themselves on the mathematical derivation of the wave diffraction. Friedlander and Taylor (1946) focuses on the interaction of a pulse and the same semi-infinite screen. In figure 2.14, the semi-infinite screen is located on the x-axis at the positive x values, while the incident pulse moves in the negative y direction.

For a normal incident wave, the waves are described as a combination of two functions which are based on function 2.8, but contain a different variation of X.

$$P(X,T) = \frac{\sqrt{X}}{\pi}\int_0^T \frac{p_0(z)}{(T+X-z)\sqrt{T-z}}dz \tag{2.26}$$

where T is a length parameter, X is described by either X_1 or X_2 and θ and r can be found from the location of the new point. :

$$\begin{aligned} X_1 &= r(1+sin(\theta)) \\ X_2 &= r(1-sin(\theta)) \\ T &= ct \\ r &= \sqrt{x^2+y^2} \\ \theta &= arctan(y/x) \end{aligned}$$

Using 2.26 and the relations described for X_1 and X_2, the diffracted pressure can be described using equation 2.27.

$$p_3 = \frac{1}{2}(P(X_1,T)+P(X_2,T)) \tag{2.27}$$

Equation 2.27 describes the diffracted pressure of a blast wave, which is based on the location of the selected point, as well as the input wave. These integrations, using the regular Friedlander equation as a blast wave, lead to the pressure time curves visible in figure 2.15.

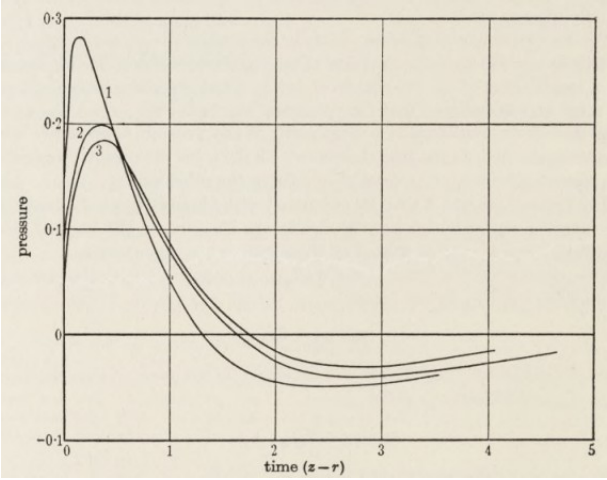

Figure 2.15: Friedlander integration results for locations given in figure 2.14

As can be seen in Figure 2.15, the waveform has changed compared to the original blast wave due to integration. The pressure time curves correspond to the locations given in figure 2.14. As can be found from figure 2.15, the change in wave shape is dependent on the location behind the wall. In figure 2.14, 3 locations were given, with increasing distance away from the wall. Location 1 shows the peak more clearly than locations 2 and 3, which are farther into the diffraction region.

Needhams approach

A second way of approximating the effects of diffraction is described by Needham (2017). This method uses the total path length between the possible blast location and subject location, which is then modified based on the diffraction angles the path is subjected to. An example of this method is displayed in figure 2.16, with a possible blast location as a circle and a subject location as a cross. As a first step, the total length is calculated using equation 2.28.

$$R_t = \sum_{i=1}^{N} R_i \tag{2.28}$$

In case of figure 2.16, this total length is the summation of R_1, R_2 and R_3. The modified length R_p used for the diffraction approximation is then calculated using each of the angles between a continuation of the path and the true loading path, shown in figure 2.16 as θ_1 and θ_2. The modified length R_p can be calculated using equation 2.29.

$$R_p = R_t * \prod_{i=1}^{N-1} sin(\theta_i + 1) \tag{2.29}$$

Using equation 2.28 and 2.29, the equivalent length for the example shown in figure 2.16 is described by equation 2.30.

$$R_p = (R_1 + R_2 + R_3) * (sin(\theta_1) + 1) * (sin(\theta_2 + 1) \tag{2.30}$$

The method by Needham describes the equivalent length, which can be used with the equivalent TNT mass to calculate the scaled distance Z, such that the Kingery Bulmash relations can be used to find the overpressure and impulse at the location of the target. For angles larger than 90 degrees or $\pi/2$ Radians, the multiplication factor should be set as 2, such that the diffraction into a backwards region is not overestimated.

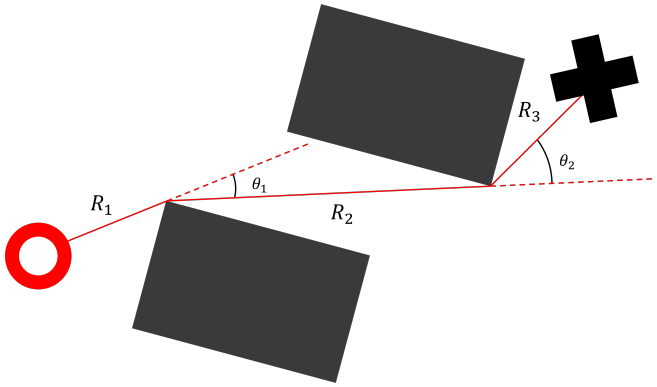

Figure 2.16: Needhams method, with the blast location as the red circle and the subject location as the cross

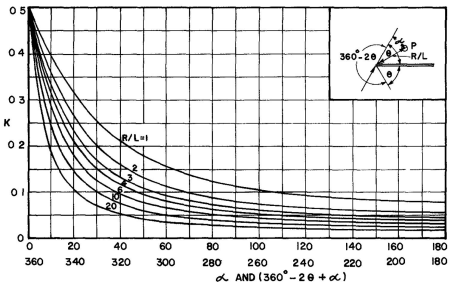

Figure 2.17: Wave diffraction coefficient (Silvester & Lim, 1968)

Exponential decay

A third option is to use an exponential decay function, which lowers the overpressure based on the angle between the blast direction and diffraction direction. The pressure can then be lowered with a factor, for which equation 2.31 is used. In equation 2.31, ϕ is the angle between the incoming wave and the diffracted wave and α and β are parameters, of which the value is based on the situation.

$$f(\phi) = \beta * \exp^{-\alpha\phi} \tag{2.31}$$

This approach stems from the interaction of ocean waves with breakwaters (Holthuijsen, 2007), which in turn is based on the work of Sommerfeld (1896). In figure 2.17, the wave height over a distance away from the breakwater is shown, which shows an exponential decay over the angle between the incoming wave and the diffracted wave.

As a first assumption, the value of β can be set as 0.5. Thus, the pressure of the shock wave propagating into the undisturbed region is taken to be half that of the original wave. This assumption does not account for the geometry of the situation with respect to α and β. However, it can be argued that the diffraction factor should be based on the possible diffraction angle. Figure 2.18 shows an example of a diffraction, where the shock wave arrives from the bottom and diffracts with an angle ϕ. The maximum potential diffraction angle is noted as ϕ_{max}, which is for this case less than 90 °, while the angle away from the edge is 90 ° or $\pi/2$. It is assumed that the pressure will distribute itself in a circular pattern around the edge. To ensure that pressure is not added as a whole, it was assumed that the total pressure in a cross-section should be 0, since pressure is not added by the edge. Therefore, it was assumed that the pressure integral over the entire angle should be zero.

The integration is split into a part towards the left and a part towards the right. Since the space away from the edge is always fully available, this leads to a β value found in 2.32.

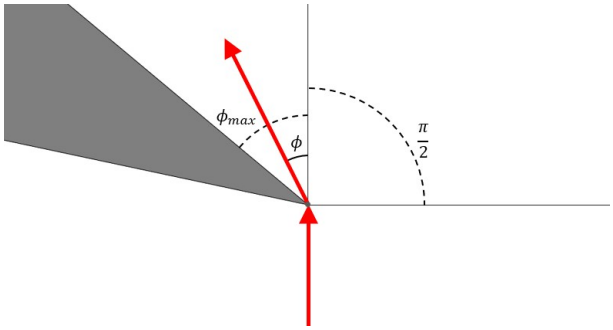

Figure 2.18: Diffraction with the diffraction angle ϕ, the maximum diffraction ϕ_{max} and the angle of away from the edge effect of $\pi/2$

$$\int_0^{\phi_{max}} \beta e^{-\alpha\phi} d\phi = \int_0^{\pi/2} (1-\beta) e^{-\alpha\phi} d\phi$$
$$\left[-\frac{\beta}{\alpha} e^{-\alpha\phi}\right]_0^{\phi_{max}} = \left[-\frac{1-\beta}{\alpha} e^{-\alpha\phi}\right]_0^{\pi/2}$$
$$\beta(1 - e^{-\alpha\phi_{max}}) = (1-\beta)\left(1 - e^{-\alpha\pi/2}\right)$$

such that

$$\beta = \frac{1 - e^{-\alpha\pi/2}}{2 - e^{-\alpha\pi/2} - e^{-\alpha\phi_{max}}} \tag{2.32}$$

However, to make use of β value found in 2.32, additional information about the geometry is needed, which was not possible in the current version of BeamBlast. Therefore, this addition is added as an improvement for future use. Therefore, in Chapter 3, where these methods are compared across experiments, a β value of 0.5 is used. This is equivalent to the assumption that the angles on both sides are equal.

In chapter 3.4.3, the three different methods of obtaining diffracted pressure will be compared with the experiment by Gabriel, Denny, Chung Kim Yuen, Langdon, and Govender, such that a best suited method can be chosen.

2.3.3. Clearing pressure

Clearing occurs when the blast wave reaches the edge of a solid finite surface, such as a wall. After the wave has been reflected, the reflected pressure of the wave will be reached, after which flow conditions establish themself around this free edge (Tyas, Bennett, Warren, Fay, & Rigby, 2011). This will result in a pressure differential, which will result in a rarefaction wave, known as the clearing wave. A simplification is shown in figure 2.19, where a wall is hit by a planar blast wave. In figure 2.19, the clearing wave is mentioned as the rarefaction wave. In this figure it is visible that while the reflecting wave returns, a black dotted wave travels from the edge to the centre of the wall, which is a pressure wave with a lower pressure than the ambient pressure. In the case of figure 2.19, the top building face and the blast wave front are parallel, which is mentioned as a zero-degree angle. The side face of the building is perpendicular to the building, which is not directly hit by the wave, and has a 90-degree angle with respect to the blast wave front. The clearing phenomenon only occurs for angles smaller than 45 degrees between surface and wave front (Rose, Smith, & May, 2006). Therefore, in the case of figure 2.19, the clearing wave only occurs in the reflected region on the top face, not on the side of the building face.

In the paper by Friedlander and Taylor (1946), the diffraction due to a semi-infinite wall has been discussed for sound waves. In this paper, it can also be noted that the clearing effects and diffraction effects occur at opposite sides of the wall, where the pressure in the region in front of the wall can be characterized by the incoming pulse, the reflected pulse due to the wall and a clearing effect, which

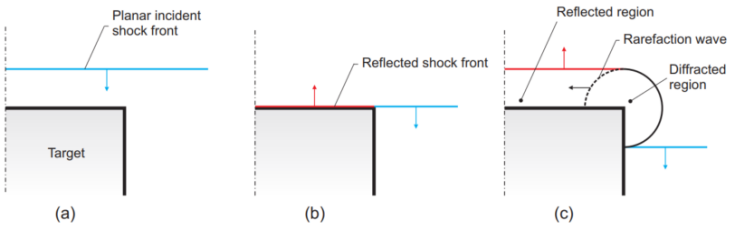

Figure 2.19: Clearing effects on a 0 degree angle (Bogosian et al., 2016)

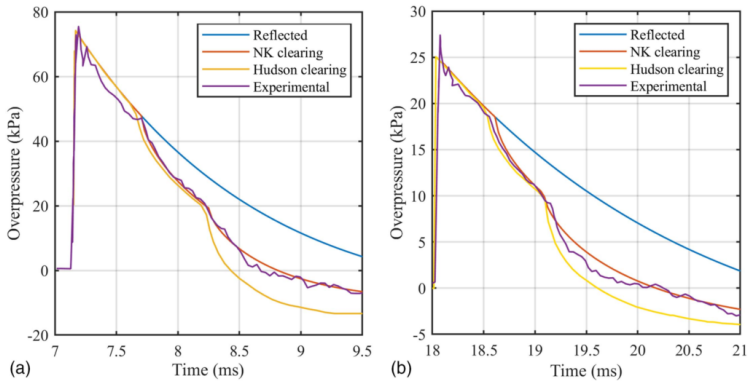

Figure 2.20: Hudson and Nartu-Kumar clearing compared to an experiment (Kumar et al., 2022)

is equal to the diffraction effect with a negative sign. Therefore, equation 2.26 can be used with the definitions for X_1 and X_2 to describe the clearing pressure, which is given in equation 2.33.

$$p_{clearing} = -\frac{1}{2}(P(X_1, T) + P(X_2, T)) \tag{2.33}$$

Other options for the clearing pressure have been compared, which are Hudson (1955) and Kumar, Kumar, and Ramisetti (2022). These two methods are shown in figure 2.20, in which it can be found that both equations are able to predict the experimental data rather well, but the NK clearing follows the experiment very closely.

2.3.4. Other edge effects

In the previous sections, the effects of a wall have been analysed in the region of the reflected, diffracted and clearing pressure regions. A number of options can be used to model the decrease in pressure in regions away from the edge faces, in contrast to the regions close to their faces. Friedlander and Taylor (1946) have not only considered the effects of a pressure wave at the front and back of a semi-infinite wall, but have also described the pressure away from the edge as well. Therefore, equation 2.26 can be used, and the equation for the pressure away from the edge can now be described by equation 2.34.

$$p(t) = -\frac{1}{2}(P(X_1, T) - P(X_2, T)) \tag{2.34}$$

Another option is to use a mirroring approach, which is shown in figure 2.21. The idea behind this is conservation, such that the total pressure of the diffracted part and edge reflected pressure is equal to the total pressure before the edge reflection. Therefore, the diffracted or clearing pressure that would occur into the direction of diffraction or clearing needs to be subtracted from the original part, which leads to the total of the pressure in the area being equal to the original blast wave. Figure 2.21 shows a representation of this approach, where there is no edge effect in the mirrored object, nor does the mirrored object have any influence on anything other than the edge effect.

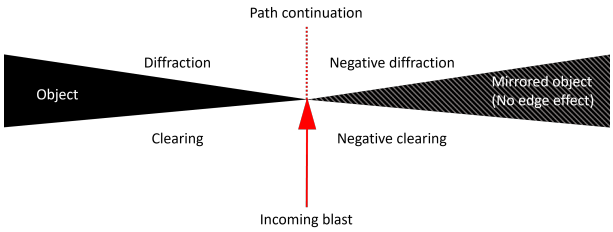

Figure 2.21: Edge effects occur in the right part, where the left part is mirrored

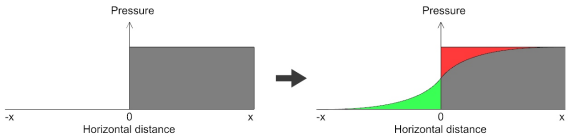

Figure 2.22: The diffracted part (green) is subtracted from the original blast wave on the left, such that the gray part on the right is the remaining blast wave. The surface of the green part is equal to that of the red part

Using this approach, the diffracted equation can be used to subtract from the original blast wave, since the idea behind this is that the total pressure behind the wall is equal to that of the incoming wave. The effect of the edge reflection pressure wave from the edge can then be described by any of the approaches mentioned in the diffraction parts. Using the notion of exponential decay, the method would be similar to figure 2.22.

For the clearing wave, 'negative' clearing wave can be applied. Quotation marks are used, since a clearing wave has a negative over-pressure by definition, such that the mirrored clearing wave is the negative wave of the clearing wave, which makes it positive. For the clearing, this means that the Friedlander equation can be applied according to 2.33, but without the negative sign.

The approach shown in figure 2.21 does however not work for all cases. When a situation similar to figure 2.23 occurs, where the blast wave hits an object directly, a different approach needs to be taken into account, since there is no ability to mirror with respect to the blast path. Considering these types of cases, an approach that can be used is to approximate an edge effect as the diffraction of a perfect reflection on the side of the edge. Therefore, the edge reflection pressure is based on the angle between the incident wall and the incident blast. Using these two, the reflected pressure is modelled. Then, the angle between a reflection and the true direction is used to calculate the reduced diffracted edge reflected wave. This approach is based on figures by Van Dyke (1982), which are shown in figure 2.23.

Although these figures do not show the pressure as a value, the radial pattern is visible. When comparing this radial pattern to figure 2.19, the same radial pattern can be found, being labelled as 'diffraction'. The radial pattern shown in figure 2.23 does not have it's origin in the edge itself and when analysing further pictures, the centre of the radial pattern seems to move in the same direction as the original blast direction. This would suggest that the radial parts away from the edge move faster, which could

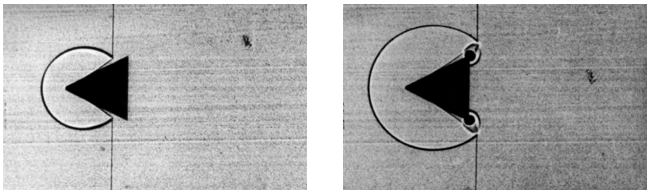

(a) (b)

Figure 2.23: Diffraction of a shock wave by a finite wedge (Van Dyke, 1982)

be explained by a higher pressure in these locations. Using this notion, the assumption was made that the pressure closer to the edge is lower, which can be modelled using the same equation as used for the diffraction for the case of exponential decay.

2.4. Predicting explosion damage

When considering building behaviour, the full load cycle can be used to estimate the damage over time. However, to be able to make an assumption of the consequences of an explosion in an early design stage, component behaviour is not yet applicable and structural behaviour might only be estimated. The pressure waves can be incredibly high, but are usually of a very short duration. Therefore, two main parameters are used for the consideration of the damage of the building. These two parameters are pressure and impulse. According to Chernin, Vilnay, Shufrin, and Cotsovos (2019), using pressure impulse diagrams are a well suited method to structural elements, such as plates, beams and shells. Such a pressure impulse curve can be found in figure 2.24.

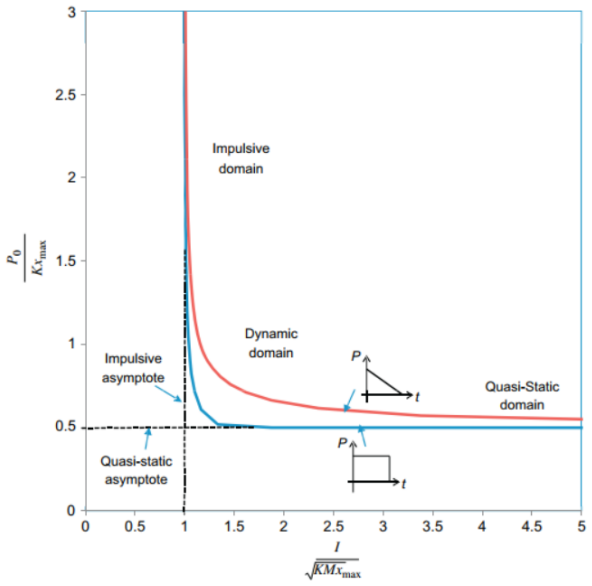

Figure 2.24: Pressure Impulse diagram (Krauthammer et al., 2008)

According to Krauthammer et al. (2008), pressure impulse curves are an easy method to determine the response to a given load. Pressure impulse curves, such as the ones shown in figure 2.24, give a failure envelope to which the pressure and impulse at each location may be given, such that damage of elements on the building facade can be approximated. Using this information, it is useful to have software that analyses blast loading to provide the impulse and pressure as outputs. Based on the type of element, the output should be given either for an area or for a multiple of points, so the load can quickly be analysed for either a new building in an existing environment or for example an existing building that could be assessed for a new situation. Then, an assessment can be made using the appropriate pressure impulse curves for the building, such that either measurements can be taken to strengthen the building or reassess a design.

Another way to simplify the loading conditions of the blast wave is by applying a Dynamic Loading Factor (DLF) to the dynamic load and applying this as a static load (VROM, 2005). This is calculated by simplifying the building as a single degree of freedom system (SDOF). The particular solution to the differential equation is found by applying the load as an impulse. The dynamic amplificcation factor is found in figure 2.25.

To find the equivalent static load on the structure, the DLF is multiplied by the maximum pressure, and is then applied on the structure. When the positive duration of the shockwave is very small compared to the natural oscillation time of the building, the DLF will be 1. In other words, the dynamic load can be considered as a static load. When the positive duration of the shockwave is closer to the natural oscillation time of the building, the DLF approaches 2.

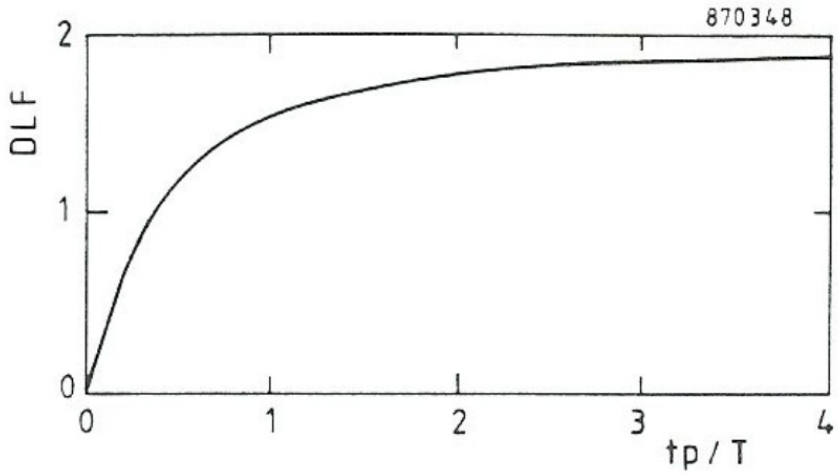

Figure 2.25: Dynamic Loading Factor for shockwaves, with positive duration of the wave t_p and natural oscillation time of the building T (VROM, 2005)

3

BeamBlast

BeamBlast is the path-based loading model that will be used in this thesis. BeamBlast has been developed by TNO (Halswijk, 2015). First, the structure and assumptions of BeamBlast will be described, such as the program flows and inputs and assumptions about reflections and edge effects. These will be described as the original version of BeamBlast, and are the original version as made by Halswijk (2015). Furthermore, this chapter will contain the additional parts that have been added to or changed within BeamBlast, referred to as the modified version. Both the original version as well as the modified version will be compared with experiments to be able to do a validation and verification of the results of BeamBlast.

3.1. Structure and input

BeamBlast has two main parts. In the first part, the geometry is defined to generate paths and make a record of the occurring edge events, such as diffraction and clearing, and surface events, such as reflections. The flow of these parts is visible in figure 3.1. The first part will shortly be mentioned below. For the second part, the 'Blast loading', the explanation has been split into two, where both the original and modified version are discussed.

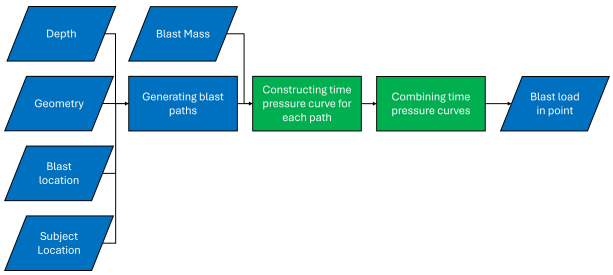

Figure 3.1: BeamBlast main parts, where blue blocks represent unchanged blocks and green blocks represent parts of the MATLAB model that have been changed for the modified version

The model has five input blocks, indicated by the parallelograms. These inputs will be explained further in chapter 3.1.1. The first four (depth, geometry, blast location and subject location) are used for the generation of blast loading paths. Within this part, the model finds the paths from the blast location to the subject location, while taking into account the geometry of the environment and by not exceeding the depth which has been set. The generation of the blast paths returns a list of paths, each with a series of events, and the corresponding location of these events. The list of events always starts at the blast location and ends at the subject location. The blast loading paths are used together with the blast mass to generate the pressure time curves for each of the paths. The time array for each of the paths is constructed with the first loading path, which is based on the arriving time and positive duration of the pressure wave. After the pressure time curves have been generated for each of the paths, the pressure time curves are added. Due to the same time array being used for all blast loading paths,

these additions are relatively straightforward.

3.1.1. Input

The input of BeamBlast contains the geometry, depth of the blast loading paths, the time over which the blast load needs to be generated and the mass of the explosive. The geometry is modelled using points and triangles. The points are modelled in 3 dimensions, after which each triangle is built by selecting the points that define the three corners of the triangle. Each triangle is then assigned to a plane, which makes the reflection in a plane possible. The blast location 'B' and subject location 'S' are defined as points in 3 dimensions. The depth is defined as a whole number, which determines the number of 'events' that can occur within a path. The mass of the explosive is defined as a number, while the time is defined as a linearly spaced list, beginning at 0, ending at a desired time, while a desired number of points between the two can be defined.

The distances in the model are defined in meters, the mass is defined in kg and the time is in seconds.

3.1.2. Path finding

This sub-section describes in short how the path-finding works. For more details, the reader is referred to Halswijk (2015). The path finding has two parts, which find the reflections and the edge effects. The path finding takes reflection into account by effectively mirroring the scene in the reflection plane and looking for a straight line in this path. The depth determines how many reflections can occur, and in effect how many reflections can occur in the scene. This mirroring assumes that the reflected path line exits the mirroring plane with the same angle as the incident path. As mentioned in chapter 2, this is true for high values of ξ, which means that the overpressure should be much smaller than the ambient pressure. Therefore, this is only correct for weak shock waves.

The edge effect path, such as clearing, diffraction and edge reflection, are determined by looking for the shortest path around an edge between two points. When an edge event occurs, this is added to the depth.

The output of the path finding are the paths that an explosion can take from the blast point 'B' to the subject 'S'. For the reflections, these paths contain information such as the triangles it occurred during its path. Considering the edge effects, the path contains information on which edge effect occurred, which line was hit, and which triangles are connected to the line. There is no specific order in which the triangles are mentioned.

The effect of increasing the depth is visible in figure 3.2. A simple situation has been modelled, with a blast at one end and a subject at the other end. Parallel to this line are two walls on both sides, on which reflections are possible. For a depth of 0, no reflections are possible, such that the only path is the direct path is from blast to subject. For a depth of 1, a single reflection is allowed, such that the path can now reflect from both the left and right wall. As can be seen in figure 3.2b, the paths with a depth less then the maximum depth are included as well. For a depth of 2, there are two reflections possible, such that the path can now reflect on the wall twice, which results in two extra paths, such that there are 5 paths in total.

3.1.3. Blast load generation

The blast loading part is the main focus of this thesis and will be explained in the next sections, but the main procedure of the approach will be explained here. For both the original, which was made by Halswijk, and the modified version, which has been altered for this thesis, the procedure is roughly the same. For each of the paths generated by the path finding, the blast load part models the pressure wave at the subject location for each of the individual parts. It does this while taking into account all events, such as reflections and edge effects. For each of the paths, a pressure wave is returned as an array of pressures based on a given time array. All of these pressure waves are added, such that a total pressure profile is generated based on the paths that have been taken into account. The peak pressure and positive impulse are returned to the user. However, the total pressure time curve can also be returned, depending on user preference.

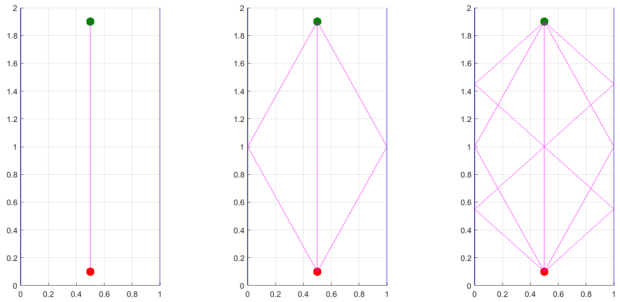

(a) Depth=0 **(b)** Depth=1 **(c)** Depth=2

Figure 3.2: The number of blast paths is based on the depth that is used

Wave parameter	Parameter description	Unit
P_{so}	Peak pressure	kPa
t_a	Arrival time	ms
t_d	Positive duration	ms
d	Decay parameter	-

Table 3.1: Wave parameters used for generation of pressure time curve in the original BeamBlast version

3.2. Original Blast Loading

This chapter will go into the structure and assumptions of the original Blast Loading script, which was made by Halswijk (2015).

3.2.1. Structure

BeamBlast starts by modelling additional parameters about the path, such as the length of the chapter and the directions of the path chapters. It then loops over the number of events for each path.

3.2.2. Reflections and edge effects

Within the loop, two parameters are updated for each iteration. These parameters are associated either with the pressure peak or the scaled distance. Within the original version of BeamBlast, the edge reflections are not taken into account and therefore produces no pressure wave. The effect of a reflection is considered by assuming that the pressure after the blast is the same as before the blast. When a point close to the surface is chosen, the reflected path and direct path arrive at the same time, such that the total pressure is equal to twice the original pressure, which is in line with a reflection factor of 2. This is only true if the depth is chosen to allow a reflected wave to arrive. Considering diffraction, the notion by Needham (2017) has been used, which assumes that the path length increases with a factor $1 + sin(\theta)$ compared to a straight line. This has been implemented by increasing the path length by $(0.5 + 0.5sin(\theta))$ when the angle between the wall and is smaller than 90 degrees. When the angle is bigger than 90 degrees, the path length is increased with a factor 2. Clearing effects have been implemented by increasing the path length of the chapter, while turning the pressure into a negative number.

3.2.3. Wave parameters

The wave parameters are found using the Kingery Bulmash relations, using the changes in terms of length. The Kingery Bulmash relations were extrapolated log-linearly, such that they could be used outside of their regular scaled distance boundaries. A warning is produced when the Kingery-Bulmash relations are used outside of their range, to warn the user of the potential inaccuracy of the result.

3.2.4. Wave shape

The wave shape is based on a modified Friedlander curve, of which the shape is based on the wave parameters. For the clearing effect, equation 3.1 is used, where p_{cl} is the clearing pressure, p_{Fl} the

Friedlander pressure, t(i) and t(i+1) the ith and (i+1)th element of the time array and t_d the positive duration.

$$p_{cl}(i+1) = p_{cl}(i) + (p_{FL}(i) - p_{cl}(i)) * \frac{t(i+1) - t(t)}{t_d/5} \tag{3.1}$$

3.3. Modified Blast Loading

This chapter will go over the changes in the BeamBlast script that have been made to accommodate the suggestions which have been done in chapter 2.

3.3.1. Structure

The loop goes over the events and alters the pressure waves based on the events that have been encountered during the path. First, an initial wave is generated, based on the scaled distance of the total path, after which the loop goes through the events that occur along the path. When no events take place, the initial wave is equal to the final wave for this particular path, which corresponds to a direct blast. When there is an event in the loop, the previous wave is taken as an input and a new blast wave is generated at the next event point, while taking account the type of event at the current point.

As mentioned in the introduction of this chapter, the path generation returns a list of events along a blast loading path. The blast path generation has not been changed for this thesis, since this was not the purpose of this thesis. For the modified BeamBlast, the script first calculates the total length of the path, after which the scaled distance Z is determined based on the total length and the mass of the explosive.

3.3.2. Wave parameters

In terms of the wave parameters, 7 parameters were used to describe the wave shape, which are shown in table 3.2.

Wave parameter	Parameter description	Unit
P_{so}	Peak pressure	kPa
t_a	Arrival time	ms
t_d	Positive duration	ms
d	Decay parameter	-
P_s^-	Negative peak pressure	kPa
t_d^-	Negative duration	kPa

Table 3.2: Wave parameters used for the generation of the pressure time curve in the modified BeamBlast version

These have already been described in chapter 2.2.1, and their description in MATLAB will shortly be treated here. The decay parameter 'd' has been described using the equations by Karlos et al. (2015), which can be applied at a scaled distance Z between 0.15 to 40. For the positive duration of the blast wave and peak pressure, the relation by Karlos et al. (2015) has been used, where both are obtained by interpolation of the values. For the negative phase of the blast wave, Department of Defense (2008) has been used to find the negative impulse and peak pressure, from which the negative duration could be found.

3.3.3. Initial phase

Initially, a pressure wave is generated. This pressure wave is generated using equation 2.10. The total length of the path is taken, which, together with the mass of the explosive, is used to find the wave parameters.

For the initial blast wave, the first and second point along the blast path are taken into account. As a first wave, the Friedlander wave is taken into account, which pressure, and positive time based on the distance of the first step along the path. This takes into account the distance from the first point to the second point as a distance and the mass of the explosive to determine the blast load parameters. This wave is generated as a pressure wave as an array, the length of which is based on a given time array.

3.3.4. Reflection
At a surface where reflection occurs, the previous wave is taken as an input for the reflection, together with the angle between the wall and the blast path. To find the reflected pressure of the wave, figure 2.12 has been used, which returned the reflection factor based on incident pressure and reflection angle. The pressure at this location is found using the paths before the reflected point. To account for blast wave decay over distance, the distance from the blast to the current and next point is taken into account. Using these two, the peak pressures are divided by each other to achieve the decay in pressure based on distance. The distance decay and reflection factor are combined to take into account both.

3.3.5. Diffraction
At a point where diffraction occurs, the angle between the arrival path and the continuing path is taken into account, together with the length of the next section of the path. The equations mentioned in section 2.3.2 were implemented in BeamBlast. For some of the methods from section 2.3.2, the diffraction angle was calculated from the path before and after the event.

3.3.6. Edge Reflection
At a point where diffraction occurs, the angle between the arrival path and the continuing path is taken into account, together with the length of the next section of the path. The equations mentioned in section 2.3.4 were implemented in BeamBlast. To use these equations, the diffraction angle was calculated from the path before and after the event.

3.3.7. Clearing
At a point where clearing occurs, the angle between the arrival path and the continuing path is taken into account, together with the length of the next chapter and the angle between the arrival path and the wall. The angle between the angle and the wall is used to determine whether clearing exists at all, since above 45 degrees, clearing pressure does not exist (Rose et al., 2006). The equations by Friedlander and Taylor (1946) have been used to generate a blast wave towards the next point. Due to the pressure vector given as a vector, integration cannot be applied. Instead of this, a summation is done, where the summation is done by averaging between the points and doing a summation of the average and the time step. This summation is used to generate the blast wave at the next time point.

3.4. Verification
The different methods have been implemented into the modified version of BeamBlast. To be able to conclude whether the results of the modified version of BeamBlast is in correspondence with experimental data and other blast tools, a number of comparisons have been made. Some of these include experimental data, while others use simplified blast tools to compare the results. The

3.4.1. Blast wave equation and scaled distances
To be able to check whether the script has a good implementation of scaled Kingery Bulmash Parameters, the outcome of a simple scenario was tested in both BeamBlast and BEC Version 6.3, for which the values are shown in table 3.3. BEC Version 6.3 is used by TNO to get a first insight into the effects of an explosion. This tool is used to model a hemispherical blast, while BeamBlast is used to model a spherical blast. To take into account this difference, the mass in the hemispherical model has been halved. A consistent mass of 1 kg has been used, which in the tool has been applied as 0.5 kg. The mass was placed at different distances to be able to test different values of z. The mass was placed at 0.5, 5 and 25 meters from the measurement location. Since the mass is consistently equal to 1 kg, the z values are 0.5, 5 and 25 $m/(kg^{1/3})$. The values that have been compared are the peak overpressure P, the positive duration t_d and the arrival time t_a.

3.4.2. Clearing pressure
To be able to verify the clearing pressure implementation, the paper by Tyas, Warren, Bennett, and Fay (2011) has been used. A 3D and front view can be seen in figure 3.3.

In the experiment by Tyas, Warren, et al. (2011), 250 g of C4 was placed at a stand-off distance of

	P [kPa]	t_d [ms]	t_a [ms]
0.5 m (Z= 0.5 $m/kg^{1/3}$):			
BeamBlast	3887	0.320	0.154
BeamBlast Original	2244	0.320	0.154
BEC	3339	0.332	0.165
5 m (Z= 5 $m/kg^{1/3}$):			
BeamBlast	31.3	3.33	9.00
BeamBlast Original	30.9	3.33	9.00
BEC	29.6	3.27	9.16
25 m (Z= 25 $m/kg^{1/3}$):			
BeamBlast	3.27	5.47	65.7
BeamBlast Original	3.27	5.47	65.7
BEC	3.34	5.32	65.7

Table 3.3: Results of Kingery Bulmash implementation

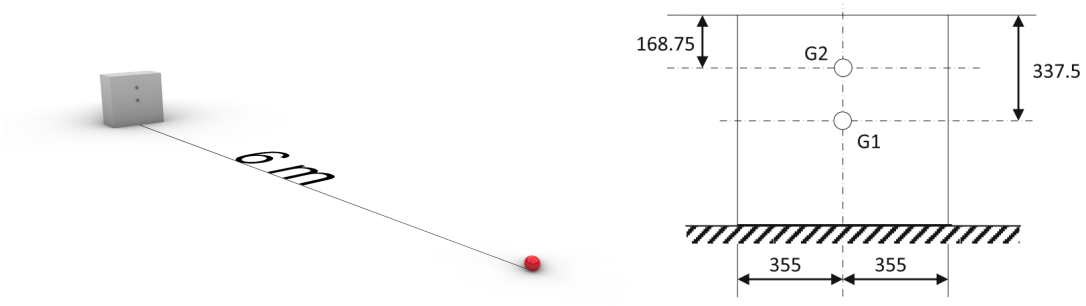

(a) 3D view of the experiment **(b)** Front view of the subject locations

Figure 3.3: Experiment by Tyas, Warren, et al. (2011)

4, 6, 8 and 10 meters. On the block, of which the front view is visible in figure 3.3.b, two pressure gauges were placed. A mass equivalence of 1.20 for C4 was used (Tyas, Warren, et al., 2011), such that the TNT equivalent mass was equal to 300 g. The 6 meter stand-off experiment was used for the verification of the models. The Hudson predictions were already done in the experiment, which are therefore not selected again in the model assumptions. For the modified version of BeamBlast, the Friedlander clearing was used. To be able to compare the results from both BeamBlast versions, the results were plotted with the results from Tyas, Warren, et al. (2011). The plots are made for a distance of 6 meters and were taken from both sensor 1 and sensor 2.

From the results in figure 3.4, it can be found that both the original and modified versions of BeamBlast predict the clearing wave at a time of 13.5 ms. These clearing waves have to take a longer path, shown in figure 3.6. For sensor 1, the distances to the top and sides are very similar (338 vs. 350 mm), leading to the 3 clearing waves arriving at a similar time. Sensor 2 is placed closer to the top of the block,

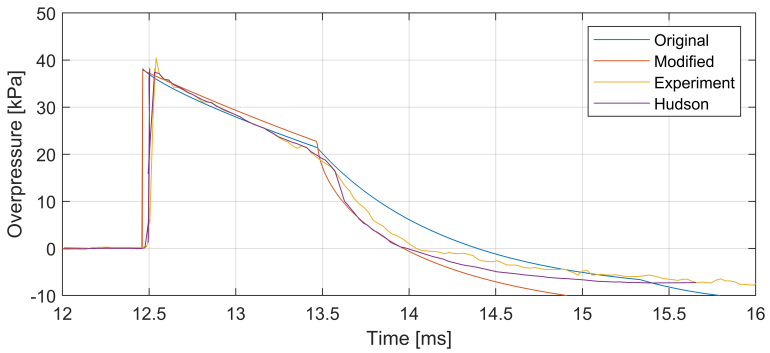

Figure 3.4: Comparing experimental data at sensor 1 at 6 meters standoff distance to BeamBlast and Hudson Clearing

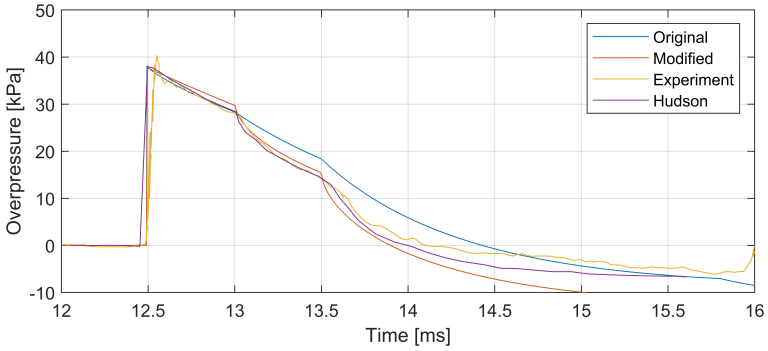

Figure 3.5: Comparing experimental data at sensor 2 at 6 meters standoff distance to BeamBlast and Hudson Clearing

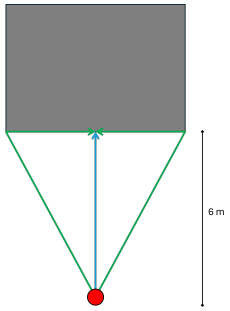

Figure 3.6: Clearing paths from BeamBlast

leading to a delay in time between the clearing waves from the top compared to the sides. The Hudson curve follows the experiment very well, while the original BeamBlast version slightly overestimates the pressure later, leading to a higher impulse. The modified BeamBlast with the Friedlander equations overestimates the negative clearing wave, leading to a lower pressure in the later stages, and a lower impulse. Similar conclusions can be drawn from figure 3.5, where the modified Friedlander equations show even lower results.

3.4.3. Diffraction

For the diffraction, a paper by Gabriel et al. (2023) has been used to study and compare the results of diffraction on a blast wave. The experiment setup is shown in figure 3.7, in which a top view is shown.

The experiment by Gabriel et al. (2023) is based on an experiment by Gajewski and Sielicki (2020). Gabriel et al. (2023) have done the experiment twice, using to different scales with respect to the original experiment by Gajewski and Sielicki. From the experiment done by Gabriel et al. (2023), the

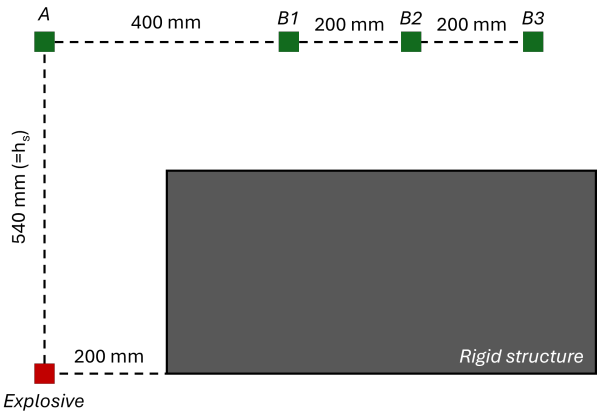

Figure 3.7: Top view of the experiment by Gabriel et al. (2023)

100% scale has been used. The explosive which has been used is PE-4, with a mass of 21.3 grams. The TNT equivalence of this explosive is 25.6 grams (Gabriel et al., 2023). The explosive has been placed on a metal bas at a height of 540 mm. The sensors, with can be found in figure 3.7 labelled as A, B1, B2 and B3, are located at a height of 540 mm as well. The distance between the explosive and the rigid structure, x_b, is equal to 200 mm. The height of the rigid block is 1080 millimetres. Two sensors were available for this experiment, of which one was placed at A for every experiment, and the other sensor was located on location B1, B2 or B3. Therefore, the pressure is measured in location A for every experiment.

This chapter compares three different methods for its verification: Friedlander, Needham and the exponential decay. To be able to compare the experiment with BeamBlast results, at all measurement locations, the peak pressure, positive duration, and arrival time were taken from Gabriel et al. (2023). The values from BeamBlast and the experiment are shown in table 3.4. The original version of Halswijk (2015) is given, together with multiple different versions of the modified BeamBlast, using the notions in section 2.3.2.

Gauge A	P_i [kPa]	t_a [ms]	t_d [ms]
Experiment (range)	254 (219-303)	0.33 (0.35-0.32)	0.58 (0.69-0.46)
BeamBlast (Original)	237	0.49	0.67
BeamBlast (Friedlander)	237	0.48	0.55
BeamBlast (Needham)	237	0.48	0.55
BeamBlast (Exp. decay)	237	0.48	0.55
Gauge B1	P_i [kPa]	t_a [ms]	t_d [ms]
Experiment (range)	69 (63-74)	0.76 (0.78-0.74)	0.46 (0.56-0.42)
BeamBlast (Original)	44.9	0.81	0.78
BeamBlast (Friedlander)	40.4	0.76	0.86
BeamBlast (Needham)	90.1	0.76	0.65
BeamBlast (Exp. decay)	67.9	0.76	0.65
Gauge B2	P_i [kPa]	t_a [ms]	t_d [ms]
Experiment (range)	37 (34-39)	1.23 (1.24-1.21)	0.64 (0.65-0.62)
BeamBlast (Original)	26.8	1.25	0.91
BeamBlast (Friedlander)	20.0	1.14	1.06
BeamBlast (Needham)	39.1	1.14	0.78
BeamBlast (Exp. decay)	41.4	1.14	0.78
Gauge B3	P_i [kPa]	t_a [ms]	t_d [ms]
Experiment (range)	31 (29-33)	1.73(1.75-1.72)	0.76 (0.78-0.73)
BeamBlast (Original)	19	1.76	1.01
BeamBlast (Friedlander)	12.2	1.60	1.16
BeamBlast (Needham)	24.9	1.60	0.87
BeamBlast (Exp. decay)	27.8	1.60	0.87

Table 3.4: Results of Gabriel et al. (2023) and the experiment modelled in different versions of BeamBlast

Considering table 3.4, the results in terms of arrival time for all three modified Beamblast versions are the same, due to the fact that they use the Kingery Bulmash relations to derive these from distance and mass. Since the Needham and Exponential decay approach do not change the wave shape, the positive duration is the same for these two. Considering the Exponential decay, equation 2.31 showed a α and β value. In section 2.3.2 it was already mentioned that a value for β can be taken as a good approach. For this experiment, the alpha was taken such that the results were similar to those in table 3.4, which was set as 0.002. However, this is based on a previously specified beta value of 0.5. Using this alpha value, the results are closer to the experimental values than the other options. Needhams approach shows a higher value for sensor B1 and B2, while showing a lower pressure for B3. The Friedlander equations show lower values, and the Friedlander equations show a much bigger positive phase compared to the experiment. Moreover, the experimental results showed a sudden peak pressure at the measured arrival time, while the Friedlander wave shows a more smooth increase in pressure, as visible in figure 2.15.

3.4.4. Edge events

Since the edge reflection is based on the same equation as both the diffraction and clearing, the edge reflection has not been verified. Although these can be checked based on experiment, it was at this stage difficult to find experiments that accurately showed the pressure based on time for a longer period. Moreover, since the negative phase of the BeamBlast results were not fully in line with the experimental results and the fact that edge effects are added to the negative part of the existing blast wave, verification has not been done on the edge events.

3.5. Discussion

Considering the peak overpressure in table 3.3, the differences are very large for lower values of Z. This is not uncommon and is mentioned by Halswijk (2015). However, it should be noted that the scaled distance where BeamBlast should be used is therefore limited between . Comparing the results for positive duration and arrival time, the results are much closer. The reason that there is a slight difference between the results from BeamBlast and the BEC is the fact that the BEC is a hemispherical calculator, while BeamBlast considers spherical explosions. Looking at the results for larger values of Z, the results from the BEC and both versions of BeamBlast are much closer.

Considering the results from the clearing procedure, all three options are able to predict the occurrence of clearing at a a relatively good point in time. The BeamBlast results are slightly early, due to the prediction of the arrival time based on the Kingery-Bulmash parameters. This causes the BeamBlast to not take into account the speed reduction due to the clearing and therefore giving an earlier arrival time. The modified BeamBlast gives a slightly higher overpressure and lower underpressure than the experimental data. When comparing the original BeamBlast results with the experiment, the results are even more clear.

The diffraction results are in a table form, which was given for the experiment. The arrival time is very different when comparing the BeamBlast results to the experiment. The low arrival time is mentioned by Gabriel et al. (2023) and explained by the use of a different explosive throughout the tests. It was explained that this should not have an effect on the other results and only occurs for the measurements for gauge A. Considering that no events take place between the blast and A, all modified results should be the same, which does occur. The positive duration of the original BeamBlast is slightly higher than both the experiment and the modified version of BeamBlast. Comparing the diffracted results, note that the exponential decay approach and Needham approach only influence the peak pressure, and not the other parameters. Therefore, both the arrival time and positive duration do not change. The peak pressure is underestimated when using the original BeamBlast as well as the Friedlander method. Considering Needhams approach, the pressure is overestimated at smaller diffraction angles, while being underestimated at larger angles. The Friedlander approach has the biggest difference, which for gauge D3, underestimates the pressure by 60 percent. The exponential decay is able to predict the diffracted pressure the best, which is caused by the fact that the α was chosen to fit this data. Therefore, when further use is wanted, these values should be looked into further, as well as improving the equation based on the notions in section 2.3.2. When looking at the results from Gabriel et al. (2023), it can be seen that although diffraction occurs, the pressure wave shows a jump in pressure when arriving. Therefore, the use of Friedlander equations for modelling diffractions is not recommended.

4

General case study

A general case has been formulated to be able to see the output when multiple effects occur at the same time and to be able to compare the results of a more complex system in BeamBlast to the results of a CFD analysis.

4.1. Physical problem

An experiment by Fouchier, Laboureur, Youinou, Lapébie, and Buchlin (2017) has been used to be able to compare the results from both types of BeamBlast as well as a CFD analysis. For this thesis, the T-Junction has been chosen as an example to be modelled. The experiment is setup on a wooden plate, with an extra metal plate in the centre with dimensions of 55 by 55 centimetre. The metal sheet is used to have better protection against the explosion. The width of the streets is equal to 250 millimetres, while the buildings have a height of 100 millimetres. Two explosives were used, both containing a mixture of pentaerythritol tetranitrate (PETN) and cyclotrimethylenetrinitramine (RDX). The explosives where positioned on the ground, making the explosions hemispherical. The experimental set-up can be seen in figure 4.1, where the explosion is shown in red and the sensors are shown in green. The walls, shown as the thick lines in figure 4.1, are built using wooden planks, which have been stacked to create a height of 100 millimetres.



Figure 4.1: Experimental set-up with the blast location in red and the sensor locations in green with the distances in millimetres

4.2. Initial conditions

For both the BeamBlast and the CFD analysis, the same mechanical model was used. It was assumed that the buildings are infinitely stiff and do not react to the explosion. Therefore, the air velocity at the building surface is equal to zero. The air pressure was assumed to be 101 hPa, while the temperature was assumed as 20 degrees celcius. For the explosives, TNT equivalents were used. According to Fouchier et al. (2017), a TNT equivalent mass of the explosives used is equal to 1.31 . It was assumed that the space behind the walls was not of much influence, which is why this space has not been

modelled for both of the analyses.

4.3. BeamBlast

In BeamBlast, the same geometries were used for both the original version and the modified version. The walls and floors are modelled as planes, which are fully reflective. Edge events can occur on the corners, such that diffraction, clearing and edge reflections are possible for these locations. The depth of the simulation was set to 3.

4.4. CFD analysis

With regards to the CFD analysis, Apollo was used as a CFD software. The advantage of Apollo compared to other software is its applicability to blast loading. Apollo uses an adaptive mesh, which creates smaller elements at the jumps in pressure, velocity and density. Further away from these jumps, the mesh size is bigger. Apollo has been used on a server within TNO, which decreases the computational time significantly. Within Apollo, the minimum block size was set to 1.25 mm, with a possibility of decreasing the block size twice. The explosive was modelled as a hemisphere. The ground and walls were modelled as fully reflective boundaries, the edge of the experiment and air were modelled as non-reflective boundaries.

4.5. Results

During the experiment, multiple sensors were used to measure the overpressure due to the explosion. Three data records were given, which are sensor 4, 8 and 10. For sensor 4, both the direct blast and the reflections are important, while for sensor 8 and 10 the diffraction and reflection are of importance. The computational time for Apollo was 1406 seconds, for the modified BeamBlast it was 1.6 seconds and for the original BeamBlast it was 0.9 seconds.

Sensor 4 experiences a direct blast and reflections from both walls, while sensors 8 and 10 experience a diffracted blast, edge effects and reflections from all walls.

Sensor 4	P_i [kPa]	t_a [ms]	t_d [ms]	I_+ [Pa s]
Experiment	120	0.41	0.58	34.8
Apollo	105	0.41	0.67	35.2
BeamBlast (original)	160	0.48	0.55	44
BeamBlast (modified)	160	0.48	0.55	44
Sensor 8	P_i [kPa]	t_a [ms]	t_d [ms]	I_+
Experiment	14	1.95	0.58	4.1
Apollo	10	1.91	0.67	3.4
BeamBlast (original)	8	2.12	0.55	2.2
BeamBlast (modified)	9	0.48	0.55	2.5
Sensor 10	P_i [kPa]	t_a [ms]	t_d [ms]	I_+
Experiment	11	3.03	0.58	3.2
Apollo	4	2.06	0.67	1.4
BeamBlast (original)	5	3.05	0.55	1.4
BeamBlast (modified)	6	0.48	0.55	1.7

Table 4.1: Results of Gabriel et al. (2023) and the experiment modelled in Apollo and BeamBlast

4.6. Discussion

When comparing the results, a large difference in the pressures can be found between the experiment and the BeamBlast results. This difference can be explained by the notion that the experiment is a ground explosion, for which the conditions can be applied in Apollo. Currently, specific conditions cannot be applied for ground explosions in BeamBlast, which causes a difference between the results. To counter these differences, an alteration could be applied to the mass, such that the results will be more in line with the experiment. However, these conditions need to be applied for any ground blast

beforehand. Another option is to implement the Kingery Bulmash relations for ground blasts. Another difference between the results is that the sensor is modelled with zero distance to the ground, which causes no reflection of the floor into the sensor. This reduces the pressure on the ground, which could be solved by either placing the sensor away from the ground for a very small amount in the BeamBlast model or by implementing the notion of a 'subject connected to surface' into BeamBlast, such that this can be taken into account in future models. Regarding the arrival time, the BeamBlast results are in line with the experimental data, as well as the positive duration. The impulse results are not in line, which can be explained by the low pressure results, causing a lower pressure time curve and therefore a lower positive impulse.

5

Urban case study

5.1. Physical problem and mechanical model

The urban case study is a fictitious situation, consisting of three buildings, which are shown in figure 5.1. The subject building, with the loaded face in green, has a height of 40 meters and a footprint of 50 by 20 meters. The other two buildings have a height of 20 meters and a footprint of 40 by 24 meters. The distance between the buildings is equal to 16 meters, equal to a two-way street with parallel parking and a pavement (Buro Sant en Co Landschapsarchitectuur, 2013). The potential blast location is located 11 meters from the face of one of the additional buildings. The possible explosion is generated by a bomb that might be placed in the rear of a small transport truck, while having a serious impact on the building. As a reference, the Oklahoma bombing was used. A TNT equivalence was based both on the drawings from the Oklahoma bombing, resulting in a TNT equivalence of 2268 kilograms, and an analysis of the seismic waves due to the explosions, resulting in a TNT equivalence of 1820 kilograms (Rogers & Koper, 2013). Considering that a transport truck is smaller than the moving truck that was used in the Oklahoma bombing (FBI, n.d.), the TNT equivalence is set as 500 kilograms.

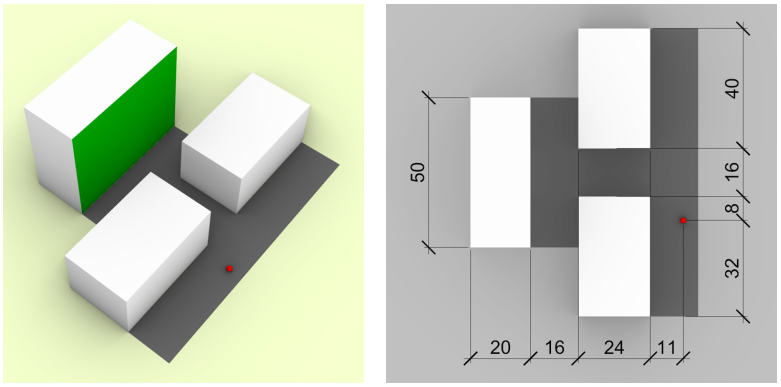

(a) 3D view of the urban case study

(b) Top down view of the urban case study (Distances in meters)

Figure 5.1: Overview of the urban case study with the blast location in red and the subject surface in dark green

This situation was chosen to create a simple geometry, which has to be modelled completely. The reason for this is that although the building composition is symmetrical, the situation is not with respect to the load. Therefore, the model can not be made smaller than its current composition, since symmetry conditions cannot be applied to a central symmetry line.

5.2. Mechanical model

The buildings are rigid structures and completely reflect the blast wave. There are no damage models, nor any dissipation of energy in the buildings. The same assumption is made for the ground. For the

properties of air, the pressure, density and temperature have to be assumed. The air temperature is assumed to be equal to 20 degrees Celcius (293 degrees Kelvin) and the air pressure is assumed to be 101 kPa. density is equal to 1.225 kg/m^3.

5.3. BeamBlast input

To be able to have an approximation of the blast load over the surface, a grid has been generated over the surface, since BeamBlast only takes into account a point blast and a point subject. The grid's edges correspond with the edges of the building, while the element size is determined by the number of elements in the direction of height and width of the building. For this analysis, the element size in both height and width of the building was equal to 5 meters, such that there are 100 elements with 121 corner points. Therefore, 121 points were analysed as a subject location to give a general idea of the pressure and impulse on the building's face. To keep the run time relatively low, the depth was set to three. The time vector was determined from the surface location, with the surface center at the same elevation as the blast as the reference point. This yields a distance of 54 meters, which, together with the mass, can be used to approximate the arrival time and the positive duration. This gives an arrival time of 125 milliseconds and a positive duration of 25 milliseconds. For the total time list, the arrival time and five times the positive duration were taken, such that the total time is 250 milliseconds.

5.4. Results

The maximum pressure and maximum positive impulse of both the original and modified BeamBlast results are shown below. In both figures, a projection of the buildings which are located in front of the wall are shown in dotted black lines. The time for the original BeamBlast analysis was 443 seconds, while the time for the modified BeamBlast was equal to 464 seconds.

Unfortunately, there are no results of an CFD analysis. This is due to the complexity of the CFD analysis and the APOLLO software, and therefore, it has not been completed in time. An analysis was attempted but was stopped after 4 hours of computational time, at which the pressure propagation was about 10% along the path from the blast location to the surface plane.

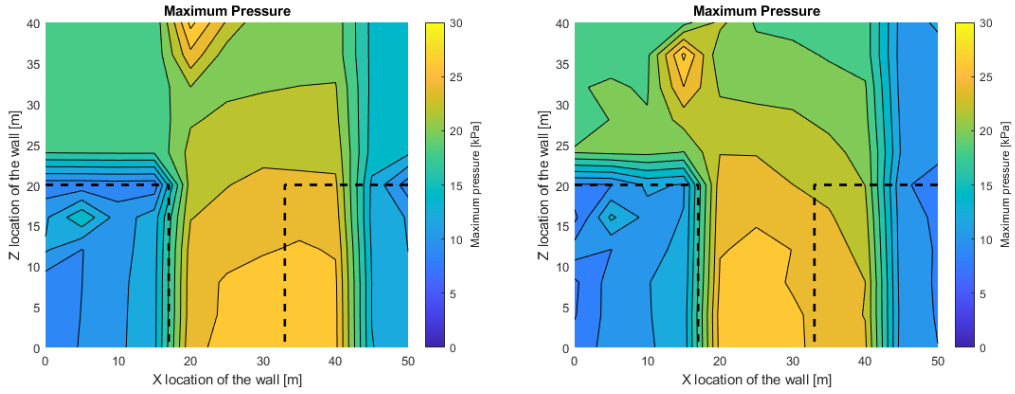

(a) Original BeamBlast version

(b) Modified BeamBlast version

Figure 5.2: Maximum overpressure for both the original and modified versions of BeamBlast, with the small buildings in front of the subject projected with the dotted lines

To be able to compare one of the points in more detail, the maximum point in figure 5.2(a) has been used as a reference $(X = 15m, Y = 36m)$. The time pressure curve is shown in figure 5.4 for this point, with both the time pressure for the original and modified versions of BeamBlast.

5.5. Discussion

When considering the maximum pressure in figure 5.2, the location of the maximum pressure is different in both cases. The highest pressure in the case of the original version of BeamBlast occurs on the far point of the right, where the blast has only diffracted once for a direct hit, and the diffraction angle is the smallest for single diffraction. Although the distance for a diffraction of a larger angle is shorter,

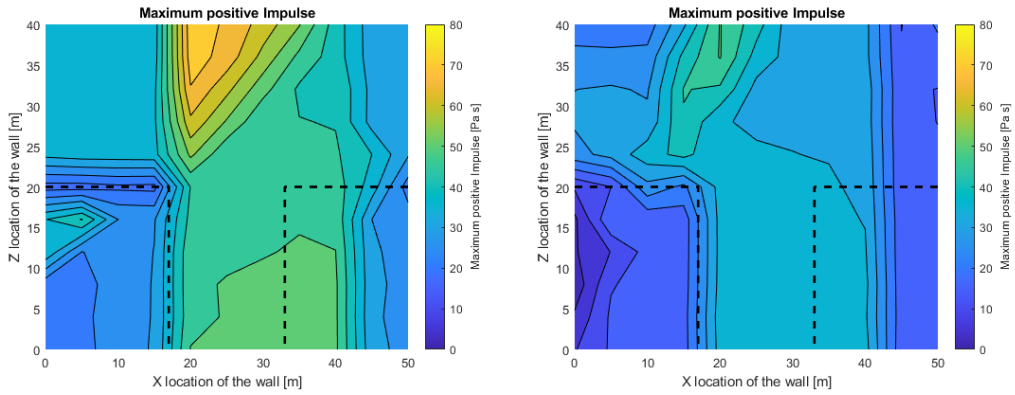

(a) Original BeamBlast version

(b) Modified BeamBlast version

Figure 5.3: Maximum positive Impulse for both the original and modified version of BeamBlast

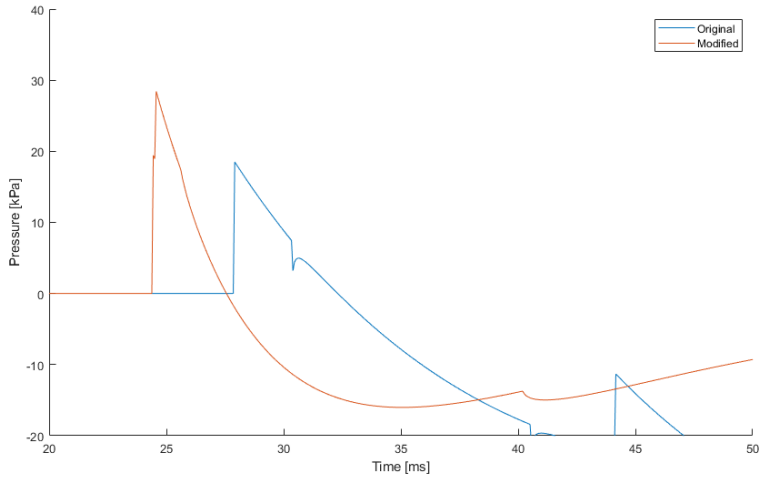

Figure 5.4: Time Pressure curves at x=15 m and y=36 m for both versions of BeamBlast

this shorter distance gets penalized by the higher diffraction angle. For the modified BeamBlast, the penalization due to diffraction is smaller, and it can be found that the highest pressure is indeed more towards the center of the building, closer to the left side of the wall.

The maximum pressure for both cases is around 40 kPa. Considering that the paths in this general case study are mainly influenced by diffraction, these results can be compared to the results found in the diffraction comparison in section 2.3.4. There, it was shown that the exponential function yielded higher pressure values than the original version of BeamBlast. Here, similar values are found for the pressure.

Similar conclusions can be found looking at the impulse in 5.3. This can be explained for the similar reasons as mentioned above, since impulse is a function of pressure and time. When looking back at section 2.3.4, the original version of BeamBlast found a higher positive duration compared to the exponential decay. Therefore, considering similar values for the pressure, a higher positive impulse will be found for the original version of BeamBlast.

From figure 5.4, the same conclusions can be found which were mentioned referring to table 3.4. There, a specific example considering diffraction was modelled in multiple versions of BeamBlast. In this case, the exponential decay function was used for the pressure, and Needham's method for the arrival time. The conclusions here is again that the arrival time of the modified version of BeamBlast is lower compared to the original version of BeamBlast. When comparing the pressure values, the modified version of BeamBlast shows higher values than the original versions, as shown in Table 3.4.

In both cases, the computational time is less than 8 minutes, which is very short. Although the comparison is difficult, the 4-hour time of the CFD software shows the difficulty of such simulations. The small difference between the two versions can be explained by the difference in clearing pressures, which each of the points on the surface experiences. Since the modified version of BeamBlast does a numerical integration over the full time, this will make the computational time longer compared to the method the original BeamBlast uses.

6

Conclusion and recommendations

6.1. Conclusion

This thesis looked into using an existing path-based loading model to approximate blast loading on buildings. It was found that the two main factors that should be communicated back to the user are the pressure and impulse of a blast wave. It has been shown that the interaction of a blast wave with edges and surfaces can be modelled using equations taking into account the geometry of the path and the surroundings. To predict the effect of clearing, numerical integration was implemented, which lowered the speed of the method. Multiple methods were tested as approaches for calculating the effect of edges, which mainly focused on the maximum overpressure, less on the positive duration and arrival time of the individual blast waves. These models were tested on experimental data of explosions in different scenarios, from which the best methods were selected for more complex analyses.

From the first of the more complex analyses, in which a T-shaped street was modelled, it was concluded that the path-based loading model, with a duration of 1 to 2 seconds, is much faster than the CFD, taking 1406 seconds. The results are comparable, but show a difference in output for close distances, since the path-based loading model was not designed for ground explosions.

From the second complex analysis, the weakness of the path-based loading model becomes more obvious. The path-based loading model determines the pressure and impulse at a chosen point, based on mass, the geometry, and the depth of the simulation. This analysis has to be done for every chosen point, such that a grid of points, which can be used to analyse a surface, takes a long time. However, for the more complex analysis, it was found that the simulation takes around 8 minutes to complete. A CFD was attempted, but was unable to run the simulation. However, a simulated distance of 10% took around four hours.

6.2. Recommendations

One of the recommendations is to look further into the diffraction equation. At this moment in time, the parameters are based on a single experiment. However, using more experimental data, the parameters could be improved, as well as the implementation of the improved equation, which was proposed in section 2. Using the improved equation, the model could be used for more complex shapes. In the current version, diffraction suffers from multiple diffractions in sequence, such as around curved corners. The improved diffraction equation takes this into account, but has not been tested.

This thesis has mainly focused on the maximum pressure and impulse. However, for some applications, the negative pressures can be very important, which this thesis has not really touched upon. It showed the negative phase and the equations, but was not focused on for the comparison of approaches or the more complex analyses.

Another improvement is to do more complex testing of the current version. It is only based on simple geometries, with less than 100 surfaces. The path based loading model could suffer from an increase in edges, due to its methods in looking for paths. However, an increased geometry could cause similar

issues for CFD software, such that it would be of importance to see how these methods compare in more complex environments.

Further research of the combination of effects is also recommended. This thesis and analyses of each of the effects mainly focussed on isolated effects, or a combination of one effect and the original blast wave. However, double effects, such as double clearing or diffraction, or the combinations of multiple different effects, such as the reflection of a clearing wave, have not been researched. Another topic is the possibility of coalescence, which was proposed to be researched but not integrated, due to time constraints.

In the introduction of this thesis, the topic of BLEVE's was mentioned as a possible sudden pressure wave, due to the transport of gases in Dutch cities. Due to the time constraints, this topic has not been researched further, but is still of interest for designers and engineers. It would be recommended to look into the possibility of using different pressure waves in the model, instead of using the TNT equivalence. It would have to be researched whether the edge effects and its approximations can still be used for lower pressure waves with a different wave form, such as deflagrations or even sound waves.

Although it is hard to compare the CFD results to those of BeamBlast, it should be noted that using a CFD software is difficult for an inexperienced user. BeamBlast and its current version are not as user friendly as it could be, the path based loading model could be improved in terms of user interface. A user only needs to input a geometry, as a list of triangles, the explosion location and mass, the subject location and the depth of the simulation to get to a full analysis. This simplifies the explosion analysis, such that a quick and simple tool for explosion prediction in complex areas could be a possibility in the future.

References

AVIV. (2021). *Rapport toetsing realisatiecijfers vervoer gevaarlijke stoffen over het spoor aan de risicoplafonds basisnet* (Tech. Rep.).

Baker, W. E. (1973). *Explosions in air*.

Bakker, P., & van Leer, B. (2019). *Lecture notes on gasdynamics, ae4-140.*

Ben-Dor, G. (2007). *Shock wave reflection phenomena* (2nd ed.). Springer Berlin, Heidelberg. doi: 10.1007/978-3-540-71382-1

Bogosian, D., Rigby, S., & Powell, D. (2016, 09). A comprehensive comparison of methods for clearing effects on reflected airblast impulse..

Buro Sant en Co Landschapsarchitectuur. (2013). *Herinrichting winkelgebied fahrenheitstraat/thomsonlaan.*

Chernin, L., Vilnay, M., Shufrin, I., & Cotsovos, D. (2019, 03). Pressure-impulse diagram method – a fundamental review. *Engineering and Computational Mechanics*, *172*. doi: 10.1680/jencm.17.00017

Department of Defense. (2008). *Ufc 3-340-02 structures to resist the effects of accidental explosions, with change 2* (Tech. Rep.).

Dewey, J. M. (2018). The friedlander equations. In I. Sochet (Ed.), *Blast effects: Physical properties of shock waves* (pp. 37–55). Cham: Springer International Publishing. doi: 10.1007/978-3-319-70831-7\textunderscore3

FBI. (n.d.). *Oklahoma city bombing.* Retrieved from `https://www.fbi.gov/history/famous-cases/oklahoma-city-bombing`

Fouchier, C., Laboureur, D., Youinou, L., Lapébie, E., & Buchlin, J.-M. (2017, 07). Experimental investigation of blast wave propagation in an urban environment. *Journal of Loss Prevention in the Process Industries*, *49*. doi: 10.1016/j.jlp.2017.06.021

Friedlander, F. G., & Taylor, G. I. (1946). The diffraction of sound pulses i. diffraction by a semi-infinite plane. *Proceedings of the Royal Society of London. Series A. Mathematical and Physical Sciences*, *186*(1006), 322-344. doi: 10.1098/rspa.1946.0046

Fuchs, B. E., Covino, J., & Baker, E. (2018, August). A critical review of tnt equivalency. In *International explosives safety symposium and exposition*.

Gabriel, S., Denny, J., Chung Kim Yuen, S., Langdon, G. S., & Govender, R. A. (2023). The effect of scaling building configuration blast experiments on positive phase blast wave parameters. *Applied Sciences*, *13*(10). Retrieved from `https://www.mdpi.com/2076-3417/13/10/5956` doi: 10.3390/app13105956

Gajewski, T., & Sielicki, P. (2020, 06). Experimental study of blast loading behind a building corner. *Shock Waves*, *30*. doi: 10.1007/s00193-020-00936-1

Glasstone, S. (1962). *The effects of nuclear weapons*. United States Atomic Energy Commission.

Granström, S. (1956). *Loading characteristics of air blasts from detonating charges*. Lindståhl. Retrieved from `https://books.google.nl/books?id=GxoblwEACAAJ`

Halswijk, W. (2015). Beamblast: a path-based blast loading model. In *16th isiems international symposium for the interaction of the effects of munitions with structures*. Retrieved from `http://resolver.tudelft.nl/uuid:36eebd6e-26be-4f7d-ae3b-e5c97a7a34d4`

Harlow, F. H., & Amsden, A. A. (1971). *Fluid dynamics*.

Holthuijsen, L. H. (2007). *Waves in oceanic and coastal waters*. Cambridge University Press.

Hopkinson, B. (1915). *British ordnance board minutes 13565*.

Hudson, C. C. (1955, 8). Sound pulse approximations to blast loading (with comments on transient drag).

James, G. M. M., Bauer, R. L., Johnson, E. M., & Johnson, C. E. (2025, May 04). Experimental determination of tnt equivalence values for binary energetic materials. *Scientific Reports*, *15*(1), 15578. Retrieved from https://doi.org/10.1038/s41598-025-99780-5 doi: 10.1038/s41598-025-99780-5

Joint Research Centre and Institute for the Protection and Security of the Citizen, Karlos, V., Viaccoz, B., & Solomos, G. (2013). *Calculation of blast loads for application to structural components*. Publications Office. doi: doi/10.2788/61866

Karlos, V., Larcher, M., & Solomos, G. (2015, 01). *Analysis of the blast wave decay coefficient in the friedlander equation using the kingery-bulmash data.*

Kenniscentrum InfoMil van Rijkswaterstaat. (2020). *Basisnet vervoer gevaarlijke stoffen'* (Tech. Rep.). Retrieved from https://www.infomil.nl/onderwerpen/veiligheid/basisnet/

Kingery, C., & Bulmash, G. (1984). *Air blast parameters from tnt spherical air burst and hemispherical surface burst*. Ballistic Research Laboratories.

Krauthammer, T., Astarlioglu, S., Blasko, J., Soh, T., & Ng, P. (2008). Pressure–impulse diagrams for the behavior assessment of structural components. *International Journal of Impact Engineering*, *35*(8), 771-783. Retrieved from https://www.sciencedirect.com/science/article/pii/S0734743X07001947 (Twenty-fifth Anniversary Celebratory Issue Honouring Professor Norman Jones on his 70th Birthday) doi: https://doi.org/10.1016/j.ijimpeng.2007.12.004

Kumar, M., Kumar, M., & Ramisetti, S. (2022, 07). Improved methodology for accurate prediction of blast wave clearing on a finite target. *Journal of Engineering Mechanics*, *148*. doi: 10.1061/(ASCE)EM.1943-7889.0002134

Lamb, H. (1906). On sommerfeld's diffraction problem. *Proceedings of the Royal Society of London*.

Ministerie", O. (n.d.). *Strafzaak explosie tarwekamp.* Retrieved from https://www.om.nl/onderwerpen/s/strafzaak-tarwekamp

Needham, C. E. (2017). *Blast waves* (2nd ed.). Springer Cham. doi: 10.1007/978-3-319-65382-2

NOS. (2023). *Vijftig wagons van goederentrein VS ontspoord, enorme vlammenzee.* Retrieved from https://nos.nl/artikel/2462477-vijftig-wagons-van-goederentrein-vs-ontspoord-enorme-vlammenzee

NOS. (2025). *Explosiegolf in Nederland houdt aan, bijna evenveel aanslagen als vorig jaar.* Retrieved from https://nos.nl/artikel/2595417-explosiegolf-in-nederland-houdt-aan-bijna-evenveel-aanslagen-als-vorig-jaar

Rigby, S. E., Tyas, A., Bennett, T., Clarke, S. D., & Fay, S. D. (2014). The negative phase of the blast load. *International Journal of Protective Structures*, *5*(1), 1-19. Retrieved from https://doi.org/10.1260/2041-4196.5.1.1 doi: 10.1260/2041-4196.5.1.1

Rogers, J. D., & Koper, K. D. (2013). *Some practical applications of forensic engineering* (Tech. Rep.). University of Missouri-Rolla.

Rose, T. A., Smith, P. D., & May, J. H. (2006, November). The interaction of oblique blast waves with buildings. *Shock Waves*, *16*(1), 35-44. doi: 10.1007/s00193-006-0051-0

Sielicki, P., & Rigby, S. (2014, 12). An investigation of tnt equivalence of hemispherical pe4 charges. *Engineering transaction*, *62*, 423-435.

Silvester, R., & Lim, T.-K. (1968, Jan.). Application of wave diffraction data. *Coastal Engineering Proceedings*, *1*(11), 16. Retrieved from https://icce-ojs-tamu.tdl.org/icce/article/view/2517 doi: 10.9753/icce.v11.16

Sommerfeld, A. (1896). Mathematische theorie der diffraction. *Mathematische Annalen*, *47*, 317-374.

Tavakoli, H., & Kiakojouri, F. (2014, Mar). Numerical dynamic analysis of stiffened plates under blast loading. *Latin American Journal of Solids and Structures*, *11*(2), 185–199. Retrieved from https://doi.org/10.1590/S1679-78252014000200003 doi: 10.1590/S1679-78252014000200003

Trouw. (2009). *LPG-trein explodeert in Italië.* Retrieved from https://www.trouw.nl/nieuws/lpg-trein-explodeert\-in-italie~b285b591/

Tyas, A., Bennett, T., Warren, J., Fay, S., & Rigby, S. (2011, 07). Clearing of blast waves on finite-sized targets – an overlooked approach. *Applied Mechanics and Materials*, *82*, 669-674. doi: 10.4028/www.scientific.net/AMM.82.669

Tyas, A., Warren, J., Bennett, T., & Fay, S. (2011, 04). Prediction of clearing effects in far-field blast loading of finite targets. *Shock Waves*, *21*, 111-119. doi: 10.1007/s00193-011-0308-0

Van Dyke, M. (1982). *An album of fluid motion* (No. dl. 2). Parabolic Press. Retrieved from https://books.google.nl/books?id=rWoeAQAAIAAJ

VROM. (2005). *Publicatiereeks gevaarlijke stoffen 1 deel 2b: Effecten van explosie op constructies* (Tech. Rep.).